Spectral methods for nonlocal wave problems

by

Marc Pillay

June, 2019

Submitted in fulfilment of the academic
requirements for the degree of
Master of Science in Applied Mathematics,
University of KwaZulu-Natal (UKZN),
School of Mathematics, Statistics and Computer Science,
Westville Campus,
Durban, 4000.

As the candidate's supervisors we have approved this thesis for submission.

Signature: _____ Name: Dr. S.K.Shindin Date: 23 \07\2019

Signature: _____ Name: Dr. N.Parumasur Date: 23 \07\2019

Preface

The work described in this dissertation was carried out in the School of Mathematics, Satistics and Computer Science at University of KwaZulu-Natal, Durban, from January 2018 to June 2019, under the supervision of Dr S.K. Shindin and Dr N. Parumasur.

This study represents original work by the author and has not otherwise been submitted in any form for any degree or diploma to any other tertiary institution. Where use has been made of the work of others, it is duly acknowledged in the text.

_____

Marc Pillay

Declaration 1 - Plagiarism

I, Marc Pillay, declare that

1. The research reported in this thesis, except where otherwise indicated, is my original research.

2. This thesis has not been submitted for any degree or examination at any other university.

3. This thesis does not contain other personal data, pictures, graphs or other information,
   unless specifically acknowledged as being sourced from other persons.

4. This thesis does not contain other persons' writing, unless specifically acknowledged as being sourced from other researchers. Where other written sources have been quoted, then:

   a. Their words have been re-written but the general information attributed to them has been referenced

   b. Where their exact words have been used, then their writing has been placed in italics and inside quotation marks, and referenced.

5. This thesis does not contain text, graphics or tables copied and pasted from the Internet, unless specifically acknowledged, and the source being detailed in the thesis and in the References sections.

Signed _____

Abstract

In this dissertation, we show that the Christov orthogonal basis allows for rapid and accurate approximations of functions, whose Fourier images develop integrable singularities at the origin. Using this result, we present an efficient Christov-type spectral method to solve the fractional nonlinear Schrödinger equation posed in the real line. The latter problem has seen a lot of development in recent years, specifically in periodic settings [4, 7, 12, 21, 38]. However, known numerical schemes do not behave well in unbounded domains. Accurate transparent boundary conditions are not available, while the only known global Hermite spectral scheme suffers from slow convergence [24]. We demonstrate that our numerical scheme has a potential to converge spectrally, provided that the Fourier images of exact solutions do not propagate singularities away from the origin. Several aspects related to the practical implementation of our scheme are discussed, its computational efficiency is demonstrated in a series of concrete simulations.

Contents

Chapter 1

Introduction

Partial differential/pseudo-differential equations in unbounded domains play an important role in modeling of various physical phenomena arising in science and engineering. In many realistic situations, exact solutions to such equations are difficult or impossible to obtain in a closed form, therefore it is natural to seek solutions numerically. This has led to the development of various numerical techniques to solve such problems. In the dissertation, we focus on one of them, commonly known in the special literature as spectral methods.

The idea of a spectral method was originally introduced in 1969 by Steven Orzag, see [9, 10, 14, 18, 31]. Spectral methods are a group of techniques which seek to write a solution of a differential equation as a finite linear combination of globally defined basis functions. The coefficients in the sum are chosen in order to satisfy the differential equation as closely as possible. The core ingredient of a spectral method is an appropriate choice of a computational basis. The latter is dictated by the concrete form of the differential equation, by its initial and boundary data and by an associated spatial domain. In many realistic applications, properly chosen computa-

tional basis yields geometric or a sub-geometric (spectral) convergence rates for the resulting spectral scheme.

In this dissertation, we focus on the study of spectral methods in context of the fractional nonlinear Schrödinger equation posed in the real line $\mathbb{R}$. The latter is given by

$$iu_t = \beta D^{2\alpha} u + \nu |u|^{2p} u, \quad x \in \mathbb{R}, \quad t \in \mathbb{R}_+, \quad u(0) = u_0, \tag{1.0.1}$$

where $D^{2\alpha}$ is the pseudo-differential operator, associated with the Fourier symbol $|\xi|^{2\alpha}$, $0 < \alpha < 1$ and $p > 0$. The equation appears in a number of plasma physics and quantum mechanics applications [13, 20, 22] and, apart from the classical case of $\alpha = 1$, has no closed form solutions. Some results related to the theoretical well-posedness analysis of model (1.0.1) are provided in [16, 22], while the numerical treatment can be found in [4, 7, 12, 21, 24, 38]. Despite some progress, problem (1.0.1) represent significant challenge from both theoretical and numerical perspectives. In [4, 7, 12, 21, 38], several methods are developed for the numerical treatment of (1.0.1). However, these methods are not suitable for simulations in the real line as, due to the non-smoothness of the Fourier symbol $|\xi|^{2\alpha}$ at the origin, exact solutions decrease at most algebraically at infinity and simple domain truncation techniques become inefficient. In many practical situations use of transparent boundary conditions, combined with an appropriate domain truncation, yields cheap and robust numerical schemes. However, such boundary conditions are not available for fractional wave equations even in a simple linear case.

The only computational algorithm that treats (1.0.1) globally in $\mathbb{R}$ is the Hermite function based spectral scheme, discussed in [24]. Unfortunately, this method cannot be very efficient for fractional values of 2α, for it is a classical fact that the Hermite expansions converge rapidly if and only if

functions under consideration decay exponentially fast at infinity (see [9]).

The latter observation is the main motivation for the research, presented in this dissertation. Instead of the Hermite basis, we propose to use Christov functions (see, e.g. [8, 11, 19, 23, 33, 36, 37] and references therein). They are intimately connected (via Fourier transform) with the classical Laguerre basis and, as demonstrated in Chapter 3, allow for rapid and accurate approximation of functions, whose Fourier images are singular at the origin and hence are particularly suitable for modeling solutions of the nonlinear fractional Schrödinger equation. Further, a simple algebraic transformation relates the Christov and the standard trigonometric functions. As a consequence, one can use the standard discrete Fast Fourier Transform (FFT) for computing the direct and the inverse discrete Christov transforms [19, 36, 37]. As demonstrated in Chapter 6, this yields very efficient practical computational schemes that are suitable for large scale simulations.

The outline of the dissertation is as follows: Chapter 4 deals with the local and global existence of solutions to the fractional Schrödinger equation. In Chapter 2, we present definitions and preliminary results from harmonic and functional analyses that are needed for our study of the rational Christov basis. In Chapter 3, we introduce the rational Christov basis, discuss its connection to the classical Laguerre basis and then derive several approximation results that are required for the analysis of our pseudospectral scheme. Chapter 5 contains a rigorous stability and convergence analyses of the Christov pseudospectral scheme, applied to the fractional nonlinear Schrödinger equation. Practical implementation of the numerical scheme as well as numerical simulations, confirming its computational efficiency, are presented in Chapter 6. Chapter 7 concludes the dissertation.

Chapter 2

Preliminaries

In this Chapter, we introduce and discuss in detail the interpolation properties of Sobolev spaces, where roughly speaking different order derivatives are integrated against different weights. The main motivation to consider such spaces is the property of the strongly continuous unitary group, associated with the fractional derivative $D^{2\alpha}$ that appears in the right-hand side of equation (1.0.1). The group is given by the Fourier multiplier, whose symbol is $e^{-i\beta|\xi|^{2\alpha}t}$. Since $0 < \alpha < 1$, it follows that the group action is not smooth in ξ near the origin. Consequently, classical solutions to (1.0.1), in general, cannot decay to zero faster than $\mathcal{O}(|x|^{-2})$ as $x \to \infty$, irrespective of the asymptotic behaviour of the input data u_0. This is a serious obstacle, as in this situation for a number of spectral methods (e.g. for Hermite and/or rational Chebyshev methods) the convergence rate is at most quadratic. It turns out that the Christov basis is free from this drawback, we have spectral convergence even when Fourier images of the solutions have square integrable discontinuities at the origin. Use of variable weight Sobolev spaces allow to express this fact in a consistent and natural way.

2.1 Notation

To begin, we fix some notation, which is used consistently throughout the dissertation.

Weighted Lebesgue spaces. Let $\Omega \subseteq \mathbb{R}$ be a measurable subset of $\mathbb{R}$ and $\omega \in L^{1,loc}(\Omega)$ be almost everywhere positive in Ω. We employ symbol

$$L^p_\omega(\Omega; B) := L^p(\Omega, \omega dx; B), \quad 1 \leq p < \infty,$$

to denote the weighted Lebesgue spaces with values in a Banach space B. In the special case of power weights $\omega_\beta(x) = |x|^\beta$, $\beta \in \mathbb{R}$, we write shortly $L^p_\beta(\Omega; B)$. When $B = \mathbb{R}$, we abbreviate $L^p_\omega(\Omega; B)$ and $L^p_\beta(\Omega; B)$ to $L^p_\omega(\Omega)$ and $L^p_\beta(\Omega)$, respectively. Finally, in all cases we omit ω if $\omega(x) = 1$.

Fourier transform. The normalized Fourier transform and its inverse are denoted by

$$\mathcal{F}[u](\xi) = \hat{u}(\xi) = \frac{1}{\sqrt{2\pi}} \int_{\mathbb{R}} e^{-i\xi x} u(x) dx,$$
$$\mathcal{F}^{-1}[\hat{u}](x) = u(x) = \frac{1}{\sqrt{2\pi}} \int_{\mathbb{R}} e^{i\xi x} \hat{u}(\xi) dx.$$

Throughout the dissertation, symbols x and ξ refer to the physical and the frequency variables, respectively.

Sobolev spaces. In the project, we make use of classical Sobolev spaces $H^\alpha(\mathbb{R})$, $\alpha \in \mathbb{R}$. These are Hilbert spaces equipped with the inner product

$$\langle u, v \rangle_{H^\alpha(\mathbb{R})} = \int_{\mathbb{R}} (1 + \xi^2)^\alpha \hat{u}(\xi) \overline{\hat{v}(\xi)} d\xi.$$

Basic properties of $H^\alpha(\mathbb{R})$ are found in [3].

Our definition of the variable weight Sobolev spaces requires the notion of the homogeneous Sobolev spaces $\mathring{H}^\alpha(\mathbb{R})$, $\alpha \in \mathbb{R}$. The homogeneous Sobolev

space $\mathring{H}^{\alpha}(\mathbb{R})$ consists of tempered distributions u, for which the following seminorm

$$\|u\|^2_{\mathring{H}^{\alpha}(\mathbb{R})} = \int_{\mathbb{R}} |\xi|^{2\alpha} |\hat{u}(\xi)|^2 d\xi$$

is finite. For $\alpha \geq \frac{1}{2}$, the seminorm $\|u\|_{\mathring{H}^{\alpha}(\mathbb{R})}$ is a norm, provided, we view elements of $\mathring{H}^{\alpha}(\mathbb{R})$ as equivalence classes modulo to polynomials in ξ of degree $n \geq 2\alpha$, see [6] for details.

2.2 Interpolation theory

Below, we cite several classical and novel results from the interpolation theory. These results are relevant for our study of weighted Bessel potential and variable weight Sobolev spaces.

2.2.1 Complex interpolation theory

Given a pair of Banach spaces $B_1 \hookrightarrow B_0$, where B_1 is continuously embedded into B_0. The main goal of the classical interpolation theory is to construct an intermediate Banach space $B_1 \hookrightarrow B' \hookrightarrow B_0$ so that the class of linear operators, bounded in B_0 and B_1, is preserved. There are several known ways to construct such an intermediate space, see the classical text [6]. In the dissertation, we employ the complex interpolation method of A. Calderon, which to every compatible pair of Banach spaces $B_1 \hookrightarrow B_0$ and a real parameter $0 < \theta < 1$, assigns an intermediate interpolation space $B_1 \hookrightarrow B' = [B_0, B_1]_{\theta} \hookrightarrow B_0$. The complex interpolation theory is a very large subject. Below, we cite three classical theorems, which we use explicitly in our calculations.

Theorem 2.2.1 ([6, Theorem 4.4.1]). *Let $A_1^i \hookrightarrow A_0^i$, $1 \leq i \leq n$ be a finite collection of compatible Banach pairs and $B_1 \hookrightarrow B_0$ be a compatible pair of*

Banach spaces. Assume $\mathcal{T}$ is a bounded n-linear map from $A_0^1 \times \cdots \times A_0^n$ to B_0 and from $A_1^1 \times \cdots \times A_1^n$ to B_1, i.e.

$$\|\mathcal{T}\|_{A_0^1 \times \cdots \times A_0^n \to B_0} = \sup_{\|u_1\|_{A_0^1} \le 1, \ldots, \|u_n\|_{A_0^n} \le 1} \|\mathcal{T}(u_1, \ldots, u_n)\|_{B_0} < \infty,$$

$$\|\mathcal{T}\|_{A_1^1 \times \cdots \times A_1^n \to B_1} = \sup_{\|u_1\|_{A_1^1} \le 1, \ldots, \|u_n\|_{A_1^n} \le 1} \|\mathcal{T}(u_1, \ldots, u_n)\|_{B_1} < \infty.$$

Then, for any $0 < \theta < 1$, $\mathcal{T}$ is bounded from $[A_0^1, A_1^1]_\theta \times \cdots \times [A_0^n, A_1^n]_\theta$ to $[B_0, B_1]_\theta$ and

$$\|\mathcal{T}\|_{[A_0^1, A_1^1]_\theta \times \cdots \times [A_0^n, A_1^n]_\theta \to [B_0, B_1]_\theta} \le \|\mathcal{T}\|^{1-\theta}_{A_1^1 \times \cdots \times A_1^n \to B_1} \|\mathcal{T}\|^{\theta}_{A_1^1 \times \cdots \times A_1^n \to B_1}.$$

Theorem 2.2.2 ([6, Theorem 5.1.2])**.** *Let $B_1 \hookrightarrow B_0$ be a compatible pair of Banach spaces. For $1 \le p_0, p_1 < \infty$ and $0 < \theta < 1$, we have*

$$[L^{p_0}(\Omega; B_0), L^{p_1}(\Omega; B_1)]_\theta = L^p(\Omega; [B_0, B_1]_\theta), \quad \tfrac{1}{p} = \tfrac{1-\theta}{p_0} + \tfrac{\theta}{p_1}.$$

Theorem 2.2.3 ([6, Theorem 5.5.3])**.** *For $1 \le p_0, p_1 < \infty$ and $0 < \theta < 1$, we have*

$$[L^{p_0}_{\omega_0}(\Omega), L^{p_1}_{\omega_1}(\Omega)]_\theta = L^p_\omega(\Omega), \quad \tfrac{1}{p} = \tfrac{1-\theta}{p_0} + \tfrac{\theta}{p_1}, \quad \omega = \omega_0^{\frac{p(1-\theta)}{p_0}} \omega_1^{\frac{p\theta}{p_1}}.$$

2.2.2 A_∞^{loc} weights

In this Chapter, we are interested in complex interpolation of weighted Sobolev-type spaces. Such results are not always available and heavily depend on the concrete weight ω, see [32]. The most general class $(A_\infty^{\mathrm{loc}})$ of admissible weights was introduced recently in [28]. It consists of all weights ω on $\mathbb{R}$, for which the following quantity

$$A_\infty^{\mathrm{loc}}(\omega; \alpha) = \sup_{[b,a] \subset \mathbb{R}, (b-a) \le 1} \Big(\sup_{I \subset [a,b], |I| \ge \alpha(b-a)} \tfrac{\omega((a,b))}{\omega(I)} \Big),$$

is finite for all $0 < \alpha < 1$. $A_\infty^{\rm loc}$ is an extension of the classical B. Muckenhoupt A_∞ class, developed in connection with one-weight strong- and weak-type inequalities for the standard Hardy-Littlewood maximal operator, see [15, 32].

We remark that $A_\infty^{\rm loc}$ class contains all power weights $\omega(x) = |x|^\beta$, $\beta > -1$ and hence is well suitable for our applications. Unfortunately, the interpolation results obtained for $A_\infty^{\rm loc}$-weights in [28] hold for Triebel-Lizorkin spaces only but in general not for the weighted Sobolev spaces. For example in Hilbert settings, the theory developed in [28] guarantees the interpolation property of Sobolev spaces with power weights $\omega(x) = |x|^\beta$ only when $-1 < \beta < 1$. The main reason for this shortcoming is the method of proof that requires local integrability of certain inverse powers of $A_\infty^{\rm loc}$-weights at the origin.

In our applications, we deal with weighted Sobolev-type spaces over positive ($\mathbb{R}_+$) and negative ($\mathbb{R}_-$) half lines. In this situation, the lack of local integrability can be avoided by considering one-sided localized analogues of the classical A_p classes. This is the main topic of the next Section.

2.3 One-sided weights and singular operators

In the dissertation, we define the variable weight Sobolev spaces in the real line in terms of weighted integrability and regularity properties of Fourier images of functions restricted to the positive $\mathbb{R}_+$ (equivalently, negative $\mathbb{R}_-$) half line. The major difficulty here is to show that for the order of regularity $\alpha \geq 0$, these spaces have an interpolation property. We remark that in the Hilbert settings, the standard weighted interpolation results hold for $-1 < \alpha < 1$ only [15, 32]. Since in the context of spectral methods the order

of regularity α can be arbitrary large, we develop an appropriate version of the theory that allows us to cover the general case. To begin, we define classes of admissible weights for which a class of maximal operators is bounded.

2.3.1 $A^{loc}_{p,\pm}(\Omega)$ weights

Our approach combines ideas of E. Sawyer [25, 30] and the localization ideas of V.S. Rychkov [28].

Let Ω be an open set in $\mathbb{R}$ and $\omega \in L^{1,loc}(\Omega)$ be an almost everywhere positive weight function in Ω. A new weight can be constructed, $\bar{\omega}_p = \omega^{-\frac{p'}{p}}$, based on ω and parameter $1 < p < \infty$. Then for some fixed $t > 0$, we define

$$[\omega]^{+}_{p,t} = \sup_{\substack{[a,b]\subset\Omega, x\in(a,b),\\ 0<|b-a|<t}} \frac{\omega^{\frac{1}{p}}([a,x])\bar{\omega}_p^{\frac{1}{p'}}([x,b])}{|b-a|}, \tag{2.3.1a}$$

$$[\omega]^{-}_{p,t} = \sup_{\substack{[a,b]\subset\Omega, x\in(a,b),\\ 0<|b-a|<t}} \frac{\bar{\omega}_p^{\frac{1}{p'}}([a,x])\omega^{\frac{1}{p}}([x,b])}{|b-a|}. \tag{2.3.1b}$$

The $A^{loc}_{p,\pm}(\Omega)$ class, with $1 < p < \infty$, consist of all almost everywhere positive locally integrable functions $\omega \in \Omega$, such that for some $t > 0$, the quantities $[\omega]^{\pm}_{p,t}$ are finite. As shown below, $A^{loc}_{p,\pm}(\Omega)$ classes are well defined, i.e. they are independent of the particular choice of the cutoff parameter $t > 0$.

Lemma 2.3.1. *Assume $\omega \in A^{loc}_{p,\pm}(\Omega)$, with $1 < p < \infty$, then $[\omega]^{\pm}_{p,t} < \infty$ for any fixed $t > 0$.*

Proof. (a) Assume $[\omega]^{+}_{p,t_0} = [\bar{\omega}_p]^{-}_{p',t_0}$ is finite. Then for any $[a,b] \subset \Omega$, with $0 < |b-a| < t_0$ and any $x \in (a,b)$, (2.3.1a), combined with Hölder's inequality, gives

$$|b-x|^p \omega([a,x]) \le ([\omega]^{+}_{p,t_0})^p |b-a|^p \omega([x,b]).$$

This allows us to conclude that

$$\big(\tfrac{|x-b|}{|b-a|}\big)^p \le \big(([\omega]^+_{p,t_0})\big)^p + 1\big)\tfrac{\omega([x,b])}{\omega([a,b])}. \tag{2.3.2a}$$

In complete analogy, formula (2.3.1b) implies

$$\big(\tfrac{|x-b|}{|b-a|}\big)^{p'} \le \big(([\bar{\omega}_p]^-_{p',t_0})^{p'} + 1\big)\tfrac{\bar{\omega}_p([x,b])}{\bar{\omega}_p([a,b])}. \tag{2.3.2b}$$

(b) Now consider an interval $[a',b'] \subset \Omega$, $0 < |b'-a'| < 2t_0$ and choose $a' < a < x_1 < b < b'$ so that $|a-a'| = |x_1-a| = |b-x_1| = |b'-b|$. By virtue of (2.3.1a) and (2.3.2), we obtain the estimate

$$\omega^{\frac{1}{p}}([a',x_1])\bar{\omega}_p^{\frac{1}{p'}}([x_1,b']) \le c'|b-a|,$$

with $c' = 4[\omega]^+_{p,t_0}(([\omega]^+_{p,t_0})^p + 1)^{\frac{1}{p}}(([\omega]^+_{p,t_0})^{p'} + 1)^{\frac{1}{p'}}$. When $x \in (a',b')$ is arbitrary, the last inequality yields

$$\omega^{\frac{1}{p}}([a',x])\bar{\omega}_p^{\frac{1}{p'}}([x,b']) \le \omega^{\frac{1}{p}}([a',x])\bar{\omega}_p^{\frac{1}{p'}}([x,x_1]) + \omega^{\frac{1}{p}}([a',x_1])\bar{\omega}_p^{\frac{1}{p'}}([x_1,b']),$$

for $a' < x < x_1$, or

$$\omega^{\frac{1}{p}}([a',x])\bar{\omega}_p^{\frac{1}{p'}}([x,b']) \le \omega^{\frac{1}{p}}([x_1,x])\bar{\omega}_p^{\frac{1}{p'}}([x_1,b']) + \omega^{\frac{1}{p}}([a',x_1])\bar{\omega}_p^{\frac{1}{p'}}([x_1,b']),$$

for $x_1 \le x < b'$. In either case, we obtain

$$\omega^{\frac{1}{p}}([a',x])\bar{\omega}_p^{\frac{1}{p'}}([x,b']) \le c''|b-a|,$$

where $c'' = [\omega]^+_{p,t_0}(1+4[\omega]^+_{p,t_0}(([\omega]^+_{p,t_0})^p+1)^{\frac{1}{p}}(([\omega]^+_{p,t_0})^{p'}+1)^{\frac{1}{p'}})$. Hence, $[\omega]^+_{p,2t_0} \le c'' < \infty$. □

Some of the basic properties of $A^{loc}_{p,\pm}(\Omega)$ are listed below:

Lemma 2.3.2 (Properties of one-sided weights)**.** *The one-sided weight classes $A^{loc}_{p,\pm}(\Omega)$, $1 < p < \infty$, satisfy:*

(i) $\omega \in A^{loc}_{p,\pm}(\Omega)$ *if and only if* $\bar{\omega}_p \in A^{loc}_{p',\mp}(\Omega)$;

(ii) if $\omega \in A^{loc}_{p,\pm}(\Omega)$, *with* $1 < p < \infty$ *and* $q > p$, *then* $\omega \in A^{loc}_{q,\pm}(\Omega)$;

(iii) for $\omega \in A^{loc}_{p,\pm}(\Omega)$ *and* $1 < p < \infty$, *we have* $\omega \in A^{loc}_{p-\epsilon,\pm}(\Omega)$ *for some* $\epsilon > 0$.

Proof. Property (i) follows directly from the definition (2.3.1). Item (ii), is the consequence of Hölder's inequality. The proof of (iii) in the non-local case of $t = \infty$ is given in [25, 30]. It's adaption to the present case is straightforward. □

2.3.2 One-sided Hardy-Littlewood maximal operators

Let Ω be an open connected subset of $\mathbb{R}$. The restricted one-sided Hardy maximal functions are defined by

$$\mathcal{M}^+_t[f](x) = \sup_{\substack{[a,b]\subset\Omega \\ 0<|b-a|<t}} \frac{1}{|b-a|}\int_x^b |f|ds, \tag{2.3.3a}$$

$$\mathcal{M}^-_t[f](x) = \sup_{\substack{[a,b]\subset\Omega \\ 0<|b-a|<t}} \frac{1}{|b-a|}\int_a^x |f|ds. \tag{2.3.3b}$$

Properties of the unrestricted ($t = \infty$) one-sided maximal operator $\mathcal{M}^{\pm}$ were investigated in great details in the paper of E. Sawyer [30], where among others the strong-type weighted $L^p_\omega(\Omega) = \left\{ f \;\middle|\; \|f\|_{L^p_\omega(\Omega)} := \|\omega^{\frac{1}{p}} f\|_{L^p(\Omega)} < \infty \right\}$, $1 \le p < \infty$, inequalities are established. In the localized case, we have

Lemma 2.3.3. *Let* $1 < p < \infty$, *the one-side maximal operators* $\mathcal{M}^{\pm}_t$ *are bounded from* $L^p_\omega(\Omega)$ *to itself, i.e.*

$$\|\mathcal{M}^{\pm}_t[f]\|_{L^p_\omega(\Omega)} \le C_{t,\omega}\|f\|_{L^p_\omega(\Omega)}, \quad t > 0, \tag{2.3.4}$$

if and only if $\omega \in A^{loc}_{p,\pm}(\Omega)$.

Proof. The proof proceeds as in the non-local case of $t = \infty$, [30]. First, one derives weak-type estimates. Then the application of the open end property (iii) from Lemma 2.3.2, combined with the classical Marcinkiewicz interpolation theorem [6], yields the result. □

2.3.3 One-sided singular integrals

In this subsection, we discuss the regular vector valued one-sided singular integrals of the form

$$\mathcal{T}_{\kappa^\mp}[f](x) = (\kappa^\mp * f)(x), \quad x \in \mathbb{R}_+, \tag{2.3.5}$$

where B_0, B_1 are two given Banach spaces, $f : \mathbb{R}_+ \to B_0$ and $\kappa^\pm(x) \in \mathcal{L}(B_0, B_1)$.[1] We assume that $\mathcal{T}_{\kappa^\mp}$ is a Calderon-Zygmund operator [32, 15], that satisfies

$$\mathcal{T}_{\kappa^\pm} \in \mathcal{L}(L^2(\mathbb{R}_+; B_0), L^2(\mathbb{R}_+; B_1)). \tag{2.3.6}$$

In our calculations, we consider compactly supported kernels only, i.e. $\operatorname{supp} \kappa^\pm \subset (-t, t) \cap \mathbb{R}_\pm$, which for all $x, y, \bar{y} \in \operatorname{supp} \kappa^\pm$, with $|x| > 0$ and $|y - \bar{y}| \leq \frac{1}{2}|x - y|$, satisfy

$$\|\kappa^\pm(x)\|_{B_0 \to B_1} \leq \frac{c}{|x|}, \tag{2.3.7a}$$

$$\|\kappa^\pm(x - y) - \kappa^\pm(x - \bar{y})\|_{B_0 \to B_1} \leq c \frac{|y - \bar{y}|}{|x - y|^2}. \tag{2.3.7b}$$

In connection with $\mathcal{T}_{\kappa^\mp}$, we define the maximal operator

$$\mathcal{M}_{\kappa^\pm}[\cdot] = \sup_{\epsilon > 0} \|\mathcal{T}_{\chi_{|x| > \epsilon} \kappa^\pm}[\cdot]\|_{B_1}. \tag{2.3.8}$$

The following lemma is an adaption of the "good-λ inequality" to the one-sided settings, [15].

[1] Here and everywhere below, $\mathcal{L}(B_1, B_2)$ denotes the space of continuous linear maps from B_1 to B_2.

Lemma 2.3.4. *Assume* $f \in L^1(\mathbb{R}_+)$ *satisfy* $\operatorname{supp} f \subset \cup_j I_j$, *where* $|I_j| < t$, $\operatorname{dist}(I_j, I_k) \geq 2t, j \neq k$. *For* $\kappa^{\pm}$ *and* $\omega \in A_\infty^{loc}$, *there exists* $0 < \alpha_\omega < 1$, *such that for any* $0 < \beta < 1$ *one can find* $\gamma > 0$ *so that the following bound holds*

$$\omega(\{\mathcal{M}_{\kappa^\pm}[f] > \xi\} \cap \{\mathcal{M}_{4t}^{\mp} \leq \gamma\xi\}) \leq \alpha_\omega(\{\mathcal{M}_{\kappa^\pm}[f] > \beta\xi\}), \tag{2.3.9}$$

for all $\xi > 0$.

Proof. (a) We consider the right-sided operators $\mathcal{M}_{\kappa^-}$ and $\mathcal{M}_t^+$ as the proof for the left-sided case is identical. Standard arguments indicate that under our assumptions on f the level set $E_{\beta\epsilon(f)} = \{\mathcal{M}_{\kappa^-}[f] > \beta\epsilon\}$ is open. The support assumption guarantees that every open connected component $I = (a, b)$ of $E_{\beta\epsilon(f)}$ satisfies $|b-a| < 2t$. It is sufficient to show (2.3.9) for a single component $I = (a, b)$, the general result follows by summation.

(b) The set $\hat{I} = I/\{\mathcal{M}_{4t}^+ > \gamma\epsilon\}$ is closed in the relative topology of I. If the Lebesgue measure of $\hat{I}$ is zero, then (2.3.9) holds trivially. So assume the measure of $\hat{I}$ is strictly positive. We let $x = \min \hat{I}$, $\hat{x} = b + (b - x)$, $f_1 = \chi_{[x,\hat{x}]} f$ and $f_2 = (1 - \chi_{[x,\hat{x}]})f$. Then

$$\omega(E_\epsilon(f) \cap I) \leq \omega(E_{\tau\epsilon}(f_1) \cap I) + \omega(E_{(1-\tau)\epsilon}(f_2) \cap I), \quad 0 < \tau < 1.$$

We estimate each term separately.

To bound $\omega(E_{\tau\epsilon}(f_1) \cap I)$, we employ the standard weak-type inequality (see [32, 15]) to obtain initially

$$|E_{\tau\epsilon}(f_1) \cap I| \leq \tfrac{c}{\tau\epsilon} \int_x^{\hat{x}} \|f\|_{B_0} dy \leq \tfrac{2c}{\tau\epsilon}|b-a|\mathcal{M}_{4t}^+[f](x) \leq \tfrac{2c\gamma}{\tau}|b-a|,$$

taking into account that $\mathcal{M}_{4t}^+[f](x) \leq \gamma\epsilon$ and $|\hat{x} - x| < 2|b-a|$. Then, using the the fact that $\omega \in A_\infty^{loc}$, we have

$$\omega(E_{\tau\epsilon}(f_1) \cap I) \leq \alpha_\omega \omega(I),$$

where $0 < \alpha_\omega < 1$, provided $0 < \gamma < 1$ is sufficiently small.

To bound $\omega(E_{(1-\tau)\epsilon}(f_2) \cap I)$, we note that in view of (2.3.7a) and (2.3.7b), for $y \in (x, b)$, we have

$$\begin{aligned}
&\|\mathcal{T}_{\kappa^-}[f_2](y) - \mathcal{T}_{\kappa^-}[f_2](b)\|_{B_1} \\
&\quad \le \int_{\hat{x}}^{b+t} \|f_2(z)\|_{B_0} \|\kappa^-(y-z) - \kappa^-(b-z)\|_{B_0 \to B_1} dz \\
&\quad \le c|y-b| \int_b^{b+t} \|f_2(z)\|_{B_0} \frac{dz}{|y-z|^2} \\
&\quad \le c \sum_{j \ge 0} 2^{-j} \big(\tfrac{2^{j+1}-1}{2^j}\big) \Big[\tfrac{1}{|r(2^{j+1}-1|)} \int_b^{b+r(2^{j+1}-1)} \chi_{[\hat{x}, b+t]} \|f_2(z)\|_{B_0} \Big] dz \\
&\quad \le 2c \sum_{j \ge 0} 2^{-j} \Big[\sup_{\substack{|b-d|>0 \\ b<d}} \frac{1}{|b-d|} \int_b^d \chi_{[b,b+t]} \|f_2(z)\|_{B_0} \Big] dz \\
&\quad \le 2c \sum_{j \ge 0} 2^{-j} \mathcal{M}_t^+[f](b) \le 4c \mathcal{M}_{4t}^+[f](b) \le 4c\gamma\epsilon,
\end{aligned}$$

where we let $r = |b - y| > 0$. Since $b \notin E_{\beta\epsilon}(f)$, taking supremum over $\epsilon > 0$, we obtain

$$\mathcal{M}_{\kappa^-}[f_2](y) \le (\beta + 4c\gamma)\epsilon \le (1-\tau)\epsilon, \quad y \in (x, b),$$

provided $0 < \gamma < 1$ is small and $0 < \tau < 1$ is chosen appropriately. Hence, $\omega(E_{(1-\tau)\epsilon}(f_2) \cap I) = 0$ and we conclude that (2.3.9) holds. □

Following a classical approach (see e.g. [15, 32]), we obtain

Lemma 2.3.5. *For $\kappa^\pm$ and $\omega \in A_{p,\mp}^{loc}(\mathbb{R}_+) \cap A_\infty^{loc}$, $1 < p < \infty$, the following bounds hold*

$$\|\mathcal{M}_{\kappa^\mp}\|_{L^p_\omega(\mathbb{R}_+; B_0) \to L^p_\omega(\mathbb{R}_+)} < \infty, \tag{2.3.10a}$$

$$\|\mathcal{T}_{\kappa^\mp}\|_{L^p_\omega(\mathbb{R}_+; B_0) \to L^p_\omega(\mathbb{R}_+; B_1)} < \infty. \tag{2.3.10b}$$

Proof. (a) First we consider $f \in C_0^\infty(\mathbb{R}_+; B_0)$. Without loss of generality, we may assume that f satisfies the support condition of Lemma 2.3.4 (as

any function is a sum of at most four functions satisfying this condition). By our assumptions, $g_\epsilon = \mathcal{T}_{\kappa^\mp \chi_{|x|>\epsilon}}[f]$ is compactly supported and smooth with $\|g_\epsilon\|_{L^\infty(\mathbb{R}_+,B_1)}$ bounded independently of $\epsilon > 0$. Since $\omega \in L^{1,loc}(\mathbb{R}_+)$, we conclude that $\|\mathcal{M}_{\kappa^\mp}[f]\|_{L^p_\omega(\mathbb{R}_+)} < \infty$. We can now use this fact together with Lemmas 2.3.4 and 2.3.3 to obtain

$$\|\mathcal{M}_{\kappa^\mp}[f]\|_{L^p_\omega(\mathbb{R}_+)} \le c\|\mathcal{M}^\pm_{4t}[f]\|_{L^p_\omega(\mathbb{R}_+)} \le c'\|f\|_{L^p_\omega(\mathbb{R}_+;B_0)},$$

for all $f \in C^\infty_0(\mathbb{R}_+;B_0)$. The standard density arguments allows one to pass from $C^\infty_0(\mathbb{R}_+;B_0)$ to $L^p_\omega(\mathbb{R}_+;B_0)$. Hence, the bound is settled.

(b) Estimate (2.3.10b) is the direct consequence of (2.3.10a), as

$$\|\mathcal{T}_{\kappa^\mp}[f]\|_{B_1} \le \mathcal{M}_{\kappa^\mp}[f] + c\|f\|_{B_0},$$

almost everywhere in $\mathbb{R}_+$, see e.g. [32]. □

2.4 Weighted Bessel potential spaces in $\mathbb{R}_\pm$

The approximation properties of the Christov basis are intimately connected with the class of weighted Bessel potential spaces in half line.

2.4.1 Definition

The weighted Bessel potential spaces $L^{p,\beta}_\omega(\mathbb{R}_\pm)$ are defined as the images of the weighted Lebesgue spaces $L^p_\omega(\mathbb{R}_\pm)$, $1 < p < \infty$, under the action of the one-sided Bessel fractional integrals [29],

$$\mathcal{J}^\beta_\mp[f](x) = [J^\beta_- * f](x), \quad J^\beta_\mp(x) = e^{\pm\frac{x}{2}}\frac{x^{\beta-1}_\mp}{\Gamma(\beta)}, \quad x_\pm = \max\{0,\pm x\}, \quad \beta > 0,$$

i.e. $L^{p,\beta}_\omega(\mathbb{R}_\pm) = \mathcal{J}^\beta_\mp[L^p_\omega(\mathbb{R}_\pm)]$.

In our study of the Bessel potential spaces with $A^{loc}_{p,\pm}(\mathbb{R}_\pm)$ weights, we require two smoothing operators. For a fixed $t > 0$ and $\varphi^\pm \in C_0^\infty(\mathbb{R})$, with $\operatorname{supp}\varphi^\pm \subset \mathbb{R}_\pm \cap (-t, t)$, we let

$$T_{\varphi^\mp,t}[f](x) = \varphi^\mp * f, \quad x \in \mathbb{R}_+.$$

Trivially, we have the bound

$$|T_{\varphi^\mp,t}[f]| \le t\|\varphi^\mp\|_\infty \mathcal{M}^\pm_t[f], \quad x \in \mathbb{R}_+.$$

For special cut-off functions $\varphi^\pm$, the estimate can be improved.

Lemma 2.4.1. *Let $\varphi \in C_0^\infty(-\frac{t}{2}, \frac{t}{2})$ be radially non-increasing. Assume $\varphi(x) = \text{const}$ for $x \in (-\frac{t}{4}, \frac{t}{4})$, $\int_{\mathbb{R}} \varphi dx = 1$ and $\varphi^\pm(\cdot) = \varphi(\pm\frac{t}{2} + \cdot)$. Then*

$$|T_{\varphi^\mp,t}[f]| \le \tfrac{3}{2}\mathcal{M}^\pm_t[f], \quad x \in \mathbb{R}_+. \tag{2.4.1}$$

Proof. Any function φ that satisfies the above conditions can be uniformly approximated from the above by step functions $\varphi_n = \sum_{i=0}^n a_i \chi_{(-t_i,t_i)}$, where $0 < a_i$, $t < 4t_i < 2t$ and $\int_{\mathbb{R}} \varphi_n dx = 1$. For such functions, we have

$$\begin{aligned} |T_{\varphi^\mp,t}[f]|(x) &\le \sum_{i=0}^n a_i \int_{\mp\frac{t}{2}-t_i}^{\mp\frac{t}{2}+t_i} |f|(x-\tau)d\tau \\ &\le \sum_{i=0}^n a_i 2t_i \frac{t+2t_i}{4t_i} \mathcal{M}^\pm_t[f](x) \le \tfrac{3}{2}\mathcal{M}^\pm_t[f](x) \end{aligned}$$

and (2.4.1) follows. □

Lemma 2.4.2. *Let $\varphi \in C_0^\infty(-\frac{t}{2}, \frac{t}{2})$ be radially non-increasing, $1 < p \le \infty$ and $\omega \in A^{loc}_{p,\pm}(\mathbb{R}_\pm)$. Then the smoothing operators $T_{\varphi^\mp,t}$ are bounded from $L^p_\omega(\mathbb{R}_\pm)$ to $L^p_\omega(\mathbb{R}_\pm)$.*

Proof. For $p = \infty$ the statement is trivial. When $1 < p < \infty$, the assertion follows from Lemmas 2.4.1 and 2.3.3. □

It was established in [29], that operators $\mathcal{J}_{\mp}^{\beta}$ are invertible for all $\beta > 0$ in the class of smooth functions defined in $\mathbb{R}_{\pm}$. We denote these inverses by $\bar{\mathcal{J}}_{\mp}^{-\beta}$. For $0 < \epsilon < 1$ and $\varphi^{\pm}$ from Lemma 2.4.1, we define $\varphi_{\epsilon}^{\pm}(\cdot) = \epsilon^{-1}\varphi^{\pm}(\epsilon^{-1}\cdot)$, $\mathcal{J}_{\epsilon,\mp}^{-\beta}[\cdot] = (\bar{\mathcal{J}}_{\mp}^{-\beta} T_{\varphi_{\epsilon}^{\mp},t})[\cdot]$ and

$$\mathcal{J}_{\mp}^{-\beta}[\cdot] = \lim_{\epsilon \to 0} \mathcal{J}_{\epsilon,\mp}^{-\beta}[\cdot],$$

where the limit is understood in $L_{\omega}^{p}(\mathbb{R}_{\pm})$ sense.

Lemma 2.4.3. *Operators $\mathcal{J}_{\mp}^{-\beta} : L_{\omega}^{p,\beta}(\mathbb{R}_{\pm}) \to L_{\omega}^{p}(\mathbb{R}_{\pm})$, $1 < p < \infty$, are one-to-one, provided that $\omega \in A_{p,\pm}^{loc}(\mathbb{R}_{\pm})$.*

Proof. We note that operators $T_{\varphi_{\epsilon}^{\mp},t}$ and $\mathcal{J}_{\mp}^{\beta}$ commute as both are defined in terms of the Fourier convolution. Therefore, for each $f \in L_{\omega}^{p,\beta}(\mathbb{R}_{\pm})$ (by definition $f = \mathcal{J}_{\mp}^{\beta}[\phi]$ for some $\phi \in L_{\omega}^{p}(\mathbb{R}_{\pm})$), we have

$$\|\mathcal{J}_{\epsilon,\mp}^{-\beta}[f] - \phi\|_{L_{\omega}^{p}(\mathbb{R}_{\pm})} = \|T_{\varphi_{\epsilon}^{\mp},t}[\phi] - \phi\|_{L_{\omega}^{p}(\mathbb{R}_{\pm})} \to 0, \quad \text{as} \quad \epsilon \to 0.$$

The conclusion follows from the uniqueness of strong limits. □

Lemma 2.4.3 implies that $\mathcal{J}_{\mp}^{\beta}$, $\beta > 0$, are isomorphisms of the scales $L_{\omega}^{p}(\mathbb{R}_{\pm})$ and $L_{\omega}^{p,\beta}(\mathbb{R}_{\pm})$, provided $1 < p \leq \infty$, $\beta > 0$ and $\omega \in A_{p,\pm}^{loc}(\mathbb{R}_{\pm})$. Hence, $L_{\omega}^{p,\beta}(\mathbb{R}_{\pm})$, $1 < p \leq \infty$, equipped with $\|\cdot\|_{L_{\omega}^{p,\beta}(\mathbb{R}_{\pm})} = \|\mathcal{J}_{\mp}^{-\beta}[\cdot]\|_{L_{\omega}^{p}(\mathbb{R}_{\pm})}$, are Banach spaces.

2.4.2 Complex interpolation

We establish the interpolation property of the weighted Bessel potential spaces $L_{\omega}^{p,\beta}(\mathbb{R}_{+})$ using an equivalent characterization of $\|\cdot\|_{L_{\omega}^{p,\beta}(\mathbb{R}_{+})}$ norm. We follow the ideas of [28], in particular, we make consistent use of the following local reproducing formula (see [28])

$$\delta = \sum_{j \leq 0} \varphi_{j}^{\pm} * \psi_{j}^{\pm}, \tag{2.4.2}$$

where δ is the delta distribution, functions $\varphi_0^{\pm}, \psi_0^{\pm} \in C_0^{\infty}(\mathbb{R})$ satisfy

$$\operatorname{supp}\varphi_0^{\pm}, \operatorname{supp}\psi_0^{\pm} \subset (-t,t)\cap\mathbb{R}_{\pm}, \quad \text{for some } t>0$$

and have non vanishing zeroth moment;

$$\varphi^{\pm}(\cdot) = \varphi_0^{\pm}(\cdot) - 2^{-1}\varphi_0^{\pm}(2^{-1}\cdot), \quad \psi^{\pm}(\cdot) = \psi_0^{\pm} - 2^{-1}\psi_0^{\pm}(2^{-1}\cdot)$$

and

$$\varphi_j^{\pm}(\cdot) = 2^j\varphi^{\pm}(2^j\cdot), \quad \psi_j^{\pm}(\cdot) = 2^j\psi^{\pm}(2^j\cdot), \quad j\geq 1.$$

Furthermore, both $\varphi_0^{\pm}$ and $\psi_0^{\pm}$ can be chosen so that

$$\int_{\mathbb{R}} x^k\varphi^{\pm}dx = \int_{\mathbb{R}} x^k\psi^{\pm}dx = 0, \quad 0\leq k\leq L, \tag{2.4.3}$$

for any given positive integer $L>0$, see [28].

For $\varphi_0^{\pm}$ as above, we define a couple of one-sided local square functions

$$\mathcal{S}^{\beta}_{\varphi^{\mp}}[f] = \Big(\sum_{j\leq 0} 2^{2j\beta}|\varphi_j^{\mp} * f|^2\Big)^{\frac{1}{2}}, \quad \beta\geq 0, \quad x\in\mathbb{R}_+.$$

Lemma 2.4.4. *For $1<p<\infty$, $\beta\geq 0$ and $\omega\in A^{loc}_{p,\pm}(\lambda)\cap A^{loc}_{\infty}$, we have*

$$\|f\|_{L^{p,\beta}_{\omega}(\mathbb{R}_+)} \approx \|\mathcal{S}^{\beta}_{\varphi^{\mp}}[f]\|_{L^p_{\omega}(\mathbb{R}_+)} \tag{2.4.4}$$

where $\approx$ means the bilateral estimate.

Proof. (a) Define $\kappa^{\pm}:\mathbb{R}_+\to\ell^2$ by means of the following formulas $\kappa^{\mp}(\cdot) = \{\varphi_j^{\mp}(\cdot)\}_{j\geq 0}$. Using the associated operator $\mathcal{T}_{\kappa^{\mp}}$, from Lemma 2.3.5, we infer

$$\|\mathcal{S}^0_{\varphi^{\mp}}[f]\| = \|\mathcal{T}_{\kappa^{\mp}}[f]\|_{L^p_{\omega}(\mathbb{R}_+;\ell^2)} \leq c\|f\|_{L^p_{\omega}(\mathbb{R}_+)}.$$

(b) The converse inequality follows from the standard duality argument and the local reproducing formula (2.4.2). Indeed, for $g\in L^{p'}_{\widetilde{\omega}_p}(\mathbb{R}_+)$ supported in $\mathbb{R}_+$, we let $g^{\pm}(\cdot) = g(\pm\cdot)$ and note that $(g^{\pm})^- = g^{\mp}$. Then

$$|\langle f,g\rangle| = |f*g^-|(0) = \big|\sum_{j\geq 0}(\varphi_j^{\mp}*f)*(\psi_j^{\mp}*g^-)\big|(0) \leq \int_{\mathbb{R}_+}\mathcal{S}^0_{\varphi^{\mp}}[f]\mathcal{S}^0_{\psi^{\pm}}[g]d\tau$$

$$\leq \|\mathcal{S}^0_{\varphi^{\mp}}[f]\|_{L^p_{\omega}(\mathbb{R}_+)}\|\mathcal{S}^0_{\psi^{\pm}}[g]\|_{L^{p'}_{\widetilde{\omega}_p}(\mathbb{R}_+)} \leq c\|\mathcal{S}^0_{\varphi^{\mp}}[f]\|_{L^p_{\omega}(\mathbb{R}_+)}\|g\|_{L^{p'}_{\widetilde{\omega}_p}(\mathbb{R}_+)}$$

and the reverse inequality follows from part (a) of the proof.

(c) The general result follows from [28, Theorem 2.18], invertibility of $\mathcal{J}_-^\beta$, Lemma 2.4.3 and (2.4.4). Indeed, consider the class

$$\bar{L}^{p,\beta}_\omega(\mathbb{R}_+) = \{f | \operatorname{supp} f \in \mathbb{R}_+, \|\mathcal{S}^\beta_{\varphi^-}[f]\|_{L^p_\omega(\mathbb{R}_+)} < \infty\}.$$

From [28, Theorem 2.18], we infer $\mathcal{J}_-^\beta[\bar{L}^{p,0}_\omega(\mathbb{R}_+)] \subset \bar{L}^{p,\beta}_\omega(\mathbb{R}_+)$, $\beta \geq 0$ and the map is onto, as $\mathcal{J}_-^\beta$ is invertible. Hence, by (2.4.4) and Lemma 2.4.3, we have $\bar{L}^{p,\beta}_\omega(\mathbb{R}_+) = \mathcal{J}_-^\beta[\bar{L}^{p,0}_\omega(\mathbb{R}_+)] = \mathcal{J}_-^\beta[L^p_\omega(\mathbb{R}_+)] = L^{p,\beta}_\omega(\mathbb{R}_+)$ as Banach spaces. □

Lemma 2.4.5. *Assume* $1 < p < \infty$ *and* $\omega_0, \omega_1 \in A^{loc}_{p,+}(\mathbb{R}_+) \cap A^{loc}_\infty$. *Then*

$$[L^{p,\beta_0}_{\omega_0}(\mathbb{R}_+), L^{p,\beta_1}_{\omega_1}(\mathbb{R}_+)]_\theta = L^{p,(1-\theta)\beta_0+\theta\beta_1}_{\omega_0^{(1-\theta)}\omega_1^\theta}(\mathbb{R}_+), \quad \beta_0, \beta_1 \geq 0, \quad \theta \in (0,1), \tag{2.4.5}$$

Proof. Directly from (2.3.1) and definition of A^{loc}_∞ weights, it follows that $\omega_0^{(1-\theta)}\omega_1^\theta \in A^{loc}_{p,+}(\mathbb{R}_+) \cap A^{loc}_\infty$, while $L^{p,\beta}_\omega(\mathbb{R}_+)$ is a retract of $L^p_\omega(\mathbb{R}_+;\ell^\beta_2)$ by Lemma 2.4.4. Consequently, direct application of Theorems 2.2.2 and 2.2.3 yields the result. □

2.5 Variable weight Sobolev space

In this section, we introduce the variable weight Sobolev spaces and investigate important properties relevant for the study of the Christov-type approximations.

2.5.1 Definition

For real valued functions, variable weight Sobolev spaces are given by

$$H^\alpha_\beta(\mathbb{R}) = \left\{u \in L^2(\mathbb{R}) \,\middle|\, \|u\|_{H^\alpha_\beta(\mathbb{R})} < \infty\right\}, \tag{2.5.1a}$$

$$\|u\|^2_{H^\alpha_\beta(\mathbb{R})} = \|u\|^2_{L^2(\mathbb{R})} + \|\hat{u}\|^2_{L^{2,\beta}_\alpha(\mathbb{R}_+)} = \|u\|^2_{L^2(\mathbb{R})} + \|\mathcal{P}_+[\kappa^-_{\beta,\ell}u]\|^2_{\mathring{H}^\alpha(\mathbb{R})}, \tag{2.5.1b}$$

where $\alpha > -\frac{1}{2}$, $\beta \geq 0$, $\kappa^{\pm}_{\beta,\ell}(x) = \frac{1}{\sqrt{2\pi}}(i\ell \pm x)^{\beta}$, are Fourier pre-images of the one-sided fractional derivatives $\mathcal{J}_{\pm}^{-\beta,\ell}[\cdot]$,

$$\mathcal{P}_{\pm}[\cdot] = \mathcal{F}^{-1}[\hat{h}_{\pm}\mathcal{F}[\cdot]], \quad \hat{h}_{\pm}(\xi) = \tfrac{1}{2}(1 \pm \operatorname{sgn}(\xi)),$$

are the projectors to the subspaces of square integrable functions that extends to an analytic function in the upper (respectively lower) half plane, $L^{2,\beta}_{\alpha}(\mathbb{R}_+)$ is the scale of Bessel potential spaces in the half-line, discussed in Section 2.4, and $\mathring{H}^{\alpha}(\mathbb{R})$ is the scale of the homogeneous Sobolev space, mentioned in Section 2.1.

2.5.2 Properties

Lemma 2.5.1. *$H^{\alpha}_{\beta}(\mathbb{R})$, with $\alpha > -\frac{1}{2}$ and $\beta \geq 0$ are Hilbert spaces. Further, if*

$$-\frac{1}{2} < \gamma \leq \alpha \leq \gamma + \beta, \quad \beta > 0, \tag{2.5.2a}$$

the following embedding holds

$$H^{\alpha}_{\beta}(\mathbb{R}) \hookrightarrow H^{\gamma}(\mathbb{R}). \tag{2.5.2b}$$

Finally, for $\alpha_0, \alpha_1 > -\frac{1}{2}$, $\beta_0, \beta_1 \geq 0$ and $\theta \in (0,1)$, we have

$$[H^{\alpha_0}_{\beta_0}(\mathbb{R}), H^{\alpha_1}_{\beta_1}(\mathbb{R})]_{\theta} = H^{(1-\theta)\alpha_0+\theta\alpha_1}_{(1-\theta)\beta_0+\theta\beta_1}(\mathbb{R}), \tag{2.5.3}$$

where $[\cdot,\cdot]_{\theta}$ is the standard complex interpolation functor of A. Calderon.

Proof. (a) It is not difficult to verify that $\|\cdot\|_{H^{\alpha}_{\beta}(\mathbb{R})}$, $\alpha > -\frac{1}{2}$, $\beta \geq 0$ is a norm in $H^{\alpha}_{\beta}(\mathbb{R})$ and that $H^{\alpha}_{\beta}(\mathbb{R})$ is complete and hence is a Banach space. The latter is the consequence of the completeness of $L^2(\mathbb{R})$ and $L^{2,\beta}_{\alpha}(\mathbb{R}_+)$. Note also $\|u\|^2_{H^{\alpha}_{\beta}(\mathbb{R})} = \langle u, u\rangle_{H^{\alpha}_{\beta}(\mathbb{R})}$, where

$$\langle u, v\rangle_{H^{\alpha}_{\beta}(\mathbb{R})} = \langle u, v\rangle_{L^2(\mathbb{R})} + \langle \mathcal{J}_{-}^{-\beta,\ell}[\hat{u}], \mathcal{J}_{-}^{-\beta,\ell}[\hat{v}]\rangle_{L^2_{\alpha}(\mathbb{R}_+)},$$

i.e. $H^{\alpha}_{\beta}(\mathbb{R})$ is a Hilbert space.

(b) The embedding (2.5.2) follows from the inequality

$$\|u\|_{L^2_\gamma(\mathbb{R}_+)} \le c\|u\|_{L^{2,\alpha}_\beta(\mathbb{R}_+)}, \tag{2.5.4}$$

which is established in [5].

(c) Interpolation identity (2.5.3) follows from Theorem 2.2.2 and the formula

$$[L^{p,\beta_0}_{\alpha_0}(\mathbb{R}_+), L^{p,\beta_1}_{\alpha_1}(\mathbb{R}_+)]_\theta = L^{p,(1-\theta)\beta_0+\theta\beta_1}_{(1-\theta)\alpha_0+\theta\alpha_1}(\mathbb{R}_+), \quad 1 < p < \infty, \tag{2.5.5}$$

(which is a particular case of (2.4.5)) if we view $H^{\alpha}_{\beta}(\mathbb{R})$ as an Euclidean space of two-element Banach valued vectors. We reiterate that for $\alpha_0 = \alpha_1 = 0$ or $\beta_0 = \beta_1 = 0$, (2.5.3) is well known. Proving (2.5.3) in general (specifically when $\alpha \notin (-1, 1)$), even in the simple case of the real line requires nontrivial constructions of Sections 2.3 and 2.4. □

We are dealing with the nonlinear Schrödinger equation containing power-type non-linearity. The convergence analysis of our numerical scheme, which we present in Chapter 5, simplifies if $H^{\alpha}_{\beta}(\mathbb{R})$ is a Banach algebra for suitable values of parameter α and β. Below, we show that this is indeed the case by checking this property explicitly for integer values of α and β. To cover fractional values of the parameters, we use the interpolation identity (2.5.3) and apply the classical multi-linear complex interpolation Theorem 2.2.1 of A. Calderon.

Lemma 2.5.2. *Assume $\alpha > \frac{1}{2}$ and $\beta \ge 0$. Then $H^{\alpha}_{\beta}(\mathbb{R})$ is a Banach algebra, i.e. for any $f, g \in H^{\alpha}_{\beta}(\mathbb{R})$*

$$\|fg\|_{H^{\alpha}_{\beta}(\mathbb{R})} \le c\|f\|_{H^{\alpha}_{\beta}(\mathbb{R})}\|g\|_{H^{\alpha}_{\beta}(\mathbb{R})}, \tag{2.5.6}$$

with $c > 0$ independent of f and g.

Proof. (a) Using the estimate $|\xi_0+\xi_1|^\alpha \le c(|\xi_0|^\alpha+|\xi_1|^\alpha)$, together with the standard Young's inequality for convolutions, for any two Hermitian functions $\hat{f},\hat{g}\in L^2_\alpha(\mathbb{R}_\pm)\cap L^2(\mathbb{R}_\pm)=L^2(\mathbb{R}_\pm,(1+|\xi|^{2\alpha})d\xi):=\bar{L}^2_\alpha(\mathbb{R}_\pm)$, we have

$$\|\hat{f}*\hat{g}\|_{L^2_\alpha(\mathbb{R}_\pm)}\le c(\|\hat{f}\|_{L^1(\mathbb{R}_\pm)}\|g\|_{L^2_\alpha(\mathbb{R}_\pm)}+\|f\|_{L^2_\alpha(\mathbb{R}_\pm)}\|\hat{g}\|_{L^1(\mathbb{R}_\pm)}).$$

By our assumption $\alpha>\frac{1}{2}$, hence after the direct application of the Hölder inequality, we obtain

$$\|\hat{f}\|_{L^1(\mathbb{R}_\pm)}\le\|(1+|\xi|^{2\alpha})^{-\frac{1}{2}}\|_{L^2(\mathbb{R}_+)}\|\hat{f}\|_{\bar{L}^2_\alpha(\mathbb{R}_\pm)}\le c\|\hat{f}\|_{\bar{L}^2_\alpha(\mathbb{R}_\pm)}$$

and we conclude

$$\|\hat{f}*\hat{g}\|_{L^2_\alpha(\mathbb{R}_\pm)}\le c\|\hat{f}\|_{\bar{L}^2_\alpha(\mathbb{R}_\pm)}\|\hat{g}\|_{\bar{L}^2_\alpha(\mathbb{R}_\pm)}.$$

(b) We let

$$\bar{L}^{2,\beta}_\alpha(\mathbb{R}_\pm)=\mathcal{J}^\beta_\mp[\bar{L}^2_\alpha(\mathbb{R}_\pm)]=L^{2,\beta}_\alpha(\mathbb{R}_\pm)\cap L^{2,\beta}_0(\mathbb{R}_\pm)$$

and observe that $\bar{L}^{2,\beta_1}_\alpha(\mathbb{R}_\pm)\hookrightarrow\bar{L}^{2,\beta_0}_\alpha(\mathbb{R}_\pm)$, whenever $0\le\beta_0\le\beta_1$, see [5]. By definition, $\mathcal{P}_++\mathcal{P}_-=\mathcal{I}$. Therefore,

$$\mathcal{P}_+[\kappa^-_{\beta,\ell}fg]=\mathcal{P}_+[\kappa^-_{\frac{\beta}{2},\ell}f]\mathcal{P}_+[\kappa^-_{\frac{\beta}{2},\ell}g]+\mathcal{P}_+[\kappa^-_{\frac{\beta}{2},\ell}f]\mathcal{P}_-[\kappa^-_{\frac{\beta}{2},\ell}g]+\mathcal{P}_-[\kappa^-_{\frac{\beta}{2},\ell}f]\mathcal{P}_+[\kappa^-_{\frac{\beta}{2},\ell}g].$$

Finally, $\kappa^-_{\frac{\beta}{2},\ell}=\sum_{i=0}^{\frac{\beta}{2}}\binom{\frac{\beta}{2}}{\ell}(2i\ell)^{\frac{\beta}{2}-i}\kappa^+_{i,\ell}$, provided $\frac{\beta}{2}$ is a positive integer. These facts combined with part (a) of the proof yields the bound

$$\begin{aligned}\|\hat{f}*\hat{g}\|_{L^{2,\beta}_\alpha(\mathbb{R}_\pm)}&\le c\sum_{i,j=0}^{\frac{\beta}{2}}\|\hat{f}\|_{\bar{L}^{2,i}_\alpha(\mathbb{R}_\pm)}\|\hat{g}\|_{\bar{L}^{2,j}_\alpha(\mathbb{R}_\pm)}\\&\le c\|\hat{f}\|_{\bar{L}^{2,\frac{\beta}{2}}_\alpha(\mathbb{R}_\pm)}\|\hat{g}\|_{\bar{L}^{2,\frac{\beta}{2}}_\alpha(\mathbb{R}_\pm)},\quad\tfrac{\beta}{2}\in\mathbb{N}.\end{aligned}\tag{2.5.7}$$

(c) We note that for any $\alpha>-\frac{1}{2}$, $\omega=1+|\xi|^{2\alpha}\in A^{loc}_{+,2}(\mathbb{R}_+)\cap A^{loc}_\infty(\mathbb{R})$, see Section 2.3. Hence,

$$[\bar{L}^{2,\beta_0}_\alpha(\mathbb{R}_+),\bar{L}^{2,\beta_1}_\alpha(\mathbb{R}_+)]_\theta=\bar{L}^{2,(1-\theta)\beta_0+\theta\beta_1}_\alpha(\mathbb{R}_+),$$

$\theta \in (0,1)$, $\beta_0, \beta_1 \geq 0$, $\alpha > -\frac{1}{2}$. Viewing the convolution product in the Fourier space as a bilinear map from $\bar{L}_\alpha^{2,\frac{\beta}{2}}(\mathbb{R}_+) \times \bar{L}_\alpha^{2,\frac{\beta_0}{2}}(\mathbb{R}_+)$ to $\bar{L}_\alpha^{2,\beta}(\mathbb{R}_+)$, $\alpha > -\frac{1}{2}$, $\beta \geq 2$ and making use of Theorem 2.2.1, we infer from (2.5.7)

$$\|\hat{f} * \hat{g}\|_{L_\alpha^{2,\beta}(\mathbb{R}_\pm)} \leq c\|\hat{f}\|_{\bar{L}_\alpha^{2,\frac{\beta}{2}}(\mathbb{R}_+)}\|\hat{g}\|_{\bar{L}_\alpha^{2,\frac{\beta}{2}}(\mathbb{R}_+)}, \quad \alpha > -\tfrac{1}{2}, \quad \beta \geq 2.$$

By virtue of (2.5.4),

$$\|\hat{f}\|_{\bar{L}_\alpha^{2,\frac{\beta}{2}}(\mathbb{R}_+)} \leq \|\hat{f}\|_{L_0^{2,\frac{\beta}{2}}(\mathbb{R}_+)} + \|\hat{f}\|_{L_\alpha^{2,\frac{\beta}{2}}(\mathbb{R}_+)} \leq c\|\hat{f}\|_{L_\alpha^{2,\frac{\beta}{2}}(\mathbb{R}_+)}, \quad 0 \leq \alpha \leq \tfrac{\beta}{2},$$

while direct application of the convolution Young's inequality in the Fourier space, followed by (2.5.4), for all $\alpha > -\frac{1}{2}$ and $\beta \geq 0$, gives

$$\begin{aligned}\|fg\|_{L^2(\mathbb{R})} &\leq c(\|f\|_{L^2(\mathbb{R})}\|\hat{g}\|_{L_\alpha^2(\mathbb{R}_\pm)} + \|\hat{f}\|_{L_\alpha^2(\mathbb{R}_\pm)}\|g\|_{L^2(\mathbb{R})}) \\ &\leq c(\|f\|_{L^2(\mathbb{R})}\|g\|_{L^2(\mathbb{R})} + \|\hat{f}\|_{L_\alpha^{2,\beta}(\mathbb{R}_\pm)}\|\hat{g}\|_{L_\alpha^{2,\beta}(\mathbb{R}_\pm)}).\end{aligned}$$

Combining the last three inequalities, we conclude that (2.5.6) holds, with $\frac{1}{2} \leq \alpha \leq \frac{\beta}{2}$ and $\beta \geq 2$.

(d) To conclude the proof we note that in the non-weighted Sobolev settings ($\beta = 0$), (2.5.6) holds for any $\alpha > \frac{1}{2}$, see [3]. Consequently combining the interpolation identity (2.5.3) and part (c) of the proof, we obtain (2.5.6) for all $\beta \geq 0$. □

Chapter 3

Approximation properties of the Christov basis

In this chapter, we introduce the Christov basis and discuss its connections with the Laguerre and the trigonometric functions. We review relevant properties of the generalized Laguerre basis function in the half-line and use them to deduce the approximation and interpolation bounds for the Christov basis functions.

3.1 The Christov basis functions

In [11], C.I. Christov introduced the following collection of functions

$$\phi_{2k}(x) = 2\,\mathrm{Im}\,\frac{(2x+i\ell)^k}{(2x-i\ell)^{k+1}} = \frac{2}{\ell}\sin(\theta)\sin((2k+1)\theta), \quad k \geq 0, \tag{3.1.1a}$$

$$\phi_{2k+1}(x) = 2\,\mathrm{Re}\,\frac{(2x+i\ell)^k}{(2x-i\ell)^{k+1}} = \frac{2}{\ell}\sin(\theta)\cos((2k+1)\theta), \quad k \geq 0, \tag{3.1.1b}$$

where $x = \frac{\ell}{2}\cot\theta$, $\theta \in [0,\pi]$. Direct calculations show

$$\langle \phi_n, \phi_m \rangle_{L^2(\mathbb{R})} = \delta_{n,m}\tfrac{\pi}{\ell}, \quad n,m \geq 0$$

and in fact the system $\{\phi_n\}_{n\geq 0}$ provides a complete orthogonal basis in $L^2(\mathbb{R})$, see [8, 11, 19, 23, 33, 36, 37]. As a consequence, any $u \in L^2(\mathbb{R})$ is represented by it's Fourier-Christov series

$$u = \tfrac{\ell}{\pi} \sum_{n\geq 0} \hat{u}_n \phi_n,$$

that converges to u in the sense of $L^2(\mathbb{R})$ and

$$\|u\|^2_{L^2(\mathbb{R})} = \tfrac{\ell}{\pi} \sum_{n\geq 0} |\hat{u}_n|^2, \quad \langle u, v\rangle_{L^2} = \tfrac{\ell}{\pi} \sum_{n\geq 0} \hat{u}_n \bar{\hat{v}}_n,$$

by the Parseval identity

The Christov basis has a number of important computational features, e.g. it follows directly from the definition (3.1.1) that ϕ_{2k} and ϕ_{2k+1}, are even, respectively odd, functions of x. The Christov and the standard trigonometric bases are connected via a simple change of variables, hence the discrete transforms can be computed efficiently via the standard Discrete Fast Fourier Transform (FFT).

The fundamental computational properties of the Christov basis are consequences of the following simple result:

Lemma 3.1.1. *The Christov functions satisfy*

$$\hat{\phi}_{2k}(\xi) = \frac{\sqrt{\pi}}{2} \varphi_k^{\ell,\alpha}(\xi), \tag{3.1.2a}$$

$$\hat{\phi}_{2k+1}(\xi) = i\,\mathrm{sgn}(\xi) \frac{\sqrt{\pi}}{2} \varphi_k^{\ell,\alpha}(\xi), \tag{3.1.2b}$$

where $\varphi_k^{\ell,\alpha}(\xi) = e^{-\frac{\ell|\xi|}{2}} L_k^{(\alpha)}(\ell|\xi|)$, $k \geq 0$, $\alpha > -1$, *are the generalized Laguerre functions.*

Proof. Formulas (3.1.2) are direct consequences of the Jordan lemma from Complex Analysis and the Calculus of Residues. □

Formulas (3.1.2), combined with the classical identities for the generalized Laguerre polynomials (see e.g. [2]), yield in particular

$$\phi'_{2k}(x) = \frac{k+1}{\ell}\phi_{2k+3} - \frac{2k+1}{\ell}\phi_{2k+1} + \frac{k}{\ell}\phi_{2k-1}, \tag{3.1.3a}$$

$$\phi'_{2k+1}(x) = -\frac{k+1}{\ell}\phi_{2k+2} + \frac{2k+1}{\ell}\phi_{2k} - \frac{k}{\ell}\phi_{2k-2}, \tag{3.1.3b}$$

for all $k \geq 0$. Identities (3.1.3) indicate that the Christov differentiation matrix is sparse (block-tridiagonal) and hence Christov-type approximations are suitable for large scale practical simulations.

3.1.1 Properties of the generalized Laguerre basis

In view of Lemma 3.1.1, the approximation properties of the Christov basis are deducible from properties of the generalized Laguerre basis in the half-line. The latter is studied in detail in [5]. Below, we cite the key result that are needed in our analysis.

The collection $\{\phi_n^\alpha(\xi)\}_{n>0}$ provides the complete orthogonal basis in the weighted Lebesgue space $L^2(\mathbb{R}_+, \xi^\alpha d\xi) := L^2_{\frac{\alpha}{2}}(\mathbb{R}_+)$. In particular, the following orthogonality relation holds (see [2])

$$\langle \phi_m^{\ell,\alpha}, \phi_k^{\ell,\alpha} \rangle_{L^2_{\frac{\alpha}{2}}(\mathbb{R}_+)} = \frac{1}{\ell^{\alpha+1}} \frac{\Gamma(k+\alpha+1)}{\Gamma(k+1)} \delta_{k,m}, \qquad k, m \geq 0 \text{ and } \alpha > -1. \tag{3.1.4}$$

With the generalized Laguerre basis, we associate the finite dimensional space $\mathbb{P}_n^\ell = \{e^{-\frac{\ell\xi}{2}}\xi^k\}_{k=0}^n$ and the family of orthogonal projectors $\mathcal{P}_n^{\ell,\alpha} : L^2_{\frac{\alpha}{2}}(\mathbb{R}_+) \to \mathbb{P}_n^\ell$, acting on the elements $u \in L^2_{\frac{\alpha}{2}}(\mathbb{R}_+)$, $\alpha > -1$, according to the formula

$$\mathcal{P}_n^{\ell,\alpha}[u] = \sum_{k=0}^{n} \tfrac{\ell^{\alpha+1}k!}{\Gamma(k+\alpha+1)} \langle u, \varphi_k^{\ell,\alpha} \rangle_{L^2_{\frac{\alpha}{2}}(\mathbb{R}_+)} \varphi_k^{\ell,\alpha}. \tag{3.1.5}$$

On the scale of weighted Bessel potential spaces the optimal errors bounds for the operators $\mathcal{P}_n^{\ell,\alpha}$ are obtained in [5].

Theorem 3.1.2 (see [5]). *Let $\alpha, \beta > -1, \gamma \geq 0$ and $\delta \geq 0$ satisfy $\beta \geq \alpha + \gamma$, $\delta \geq \beta - \alpha$. Then*

$$\|(I - \mathcal{P}_N^\alpha) f\|_{H^\gamma_{\frac{\beta}{2}}(\mathbb{R}_+)} \leq c N^{\frac{(\beta-\alpha-\delta)}{2}} \|f\|_{H^\delta_{\frac{\alpha+\delta}{2}}(\mathbb{R}_+)}, \tag{3.1.6}$$

where $c > 0$ does not depend on N or f.

3.2 Approximation error bounds

We denote $\mathbb{P}_n = \text{span}\{\phi_i\}_{i=0}^n$ and define the orthogonal projector $\mathcal{P}_n : L^2(\mathbb{R}) \to \mathbb{P}_n$, whose action on elements $u \in L^2(\mathbb{R})$ is given explicitly by the formula

$$\mathcal{P}_n[u] = \tfrac{\ell}{\pi} \sum_{k \geq 0}^{n} \hat{u}_k \phi_k.$$

From the standard theory of Hilbert spaces, we have $\lim_{n\to\infty} \|\mathcal{P}_n[u] - u\|_{L^2} = 0$. The problem is to estimate the convergence rate of the last expression. For regular functions, we have

Lemma 3.2.1. *Assume $0 \leq 2\alpha < \beta$ and $u \in H^\beta_\beta(\mathbb{R})$, then*

$$\|(I - \mathcal{P}_n)[u]\|_{H^\alpha(\mathbb{R})} \leq c\big(\tfrac{n}{2}\big)^{\alpha - \frac{\beta}{2}} \|u\|_{H^\beta_\beta(\mathbb{R})}, \tag{3.2.1}$$

where $c > 0$ does not depend on n and/or u.

Proof. The approximation error is given explicitly by

$$\|(I - \mathcal{P}_n)[u]\|^2_{L^2(\mathbb{R})} = \tfrac{\ell}{\pi} \sum_{k > n} |\hat{u}_k|^2.$$

Since the Fourier transform is an isometry from $L^2(\mathbb{R})$ to itself, we have

$$\hat{u}_k = \langle u, \phi_k \rangle = \langle \hat{u}, \hat{\phi}_k \rangle = \int_{\mathbb{R}} \hat{u}(\xi) \overline{\hat{\phi}_k(\xi)} d\xi.$$

Since $u(x)$ is real, the Fourier image $\hat{u}(\xi)$ is Hermitian, i.e. $\operatorname{Re}\hat{u}(\xi) = \operatorname{Re}\hat{u}(-\xi)$ and $\operatorname{Im}\hat{u}(\xi) = -\operatorname{Im}\hat{u}(-\xi)$. It follows from (3.1.2) that,

$$\hat{u}_{2k} = \langle u, \phi_{2k}\rangle = \langle \operatorname{Re}\hat{u}, \hat{\phi}_{2k}\rangle = \sqrt{2\pi}\int_{\mathbb{R}_+} \operatorname{Re}\hat{u}(\xi)\varphi_k^{\ell,0}(\xi)d\xi,$$

$$\hat{u}_{2k+1} = \langle u, \phi_{2k+1}\rangle = \langle \operatorname{Im}\hat{u}, \hat{\phi}_{2k+1}\rangle = \sqrt{2\pi}\int_{\mathbb{R}_+} \operatorname{Im}\hat{u}(\xi)\varphi_k^{\ell,0}(\xi)d\xi.$$

The last two formulas imply

$$\begin{aligned}\tfrac{1}{2}\|(I-\mathcal{P}_n)[u]\|^2_{H^\alpha(\mathbb{R})} = &\left\|\big(\mathcal{I}-\mathcal{P}^{\ell,0}_{\lfloor\frac{n}{2}\rfloor}\big)[\operatorname{Re}\hat{u}]\right\|^2_{L^2(\mathbb{R}_+)} + \left\|\big(\mathcal{I}-\mathcal{P}^{\ell,0}_{\lfloor\frac{n-1}{2}\rfloor}\big)[\operatorname{Im}\hat{u}]\right\|^2_{L^2(\mathbb{R}_+)}\\ &+\left\|\big(\mathcal{I}-\mathcal{P}^{\ell,0}_{\lfloor\frac{n}{2}\rfloor}\big)[\operatorname{Re}\hat{u}]\right\|^2_{L^2_\alpha(\mathbb{R}_+)} + \left\|\big(\mathcal{I}-\mathcal{P}^{\ell,0}_{\lfloor\frac{n-1}{2}\rfloor}\big)[\operatorname{Im}\hat{u}]\right\|^2_{L^2_\alpha(\mathbb{R}_+)}.\end{aligned}$$

Hence, in view of Theorem 3.1.2, we have (3.2.1). □

3.3 Interpolation error bounds

In practical calculations, we replace the exact $L^2(\mathbb{R})$ inner products with their quadrature approximations

$$\langle u, v\rangle \approx \langle u, v\rangle_n = \tfrac{\pi}{2\ell(n+1)}\sum_{j=0}^{n}(\ell^2+4x_j^2)u(x_j)\overline{v(x_j)}, \quad 0\le k\le n, \tag{3.3.1a}$$

where the nodes are given explicitly by

$$x_j = \tfrac{\ell}{2}\cot\big(\tfrac{2j+1}{2(n+1)}\pi\big), \quad 0\le j\le n. \tag{3.3.1b}$$

Direct calculations show that the discrete inner product (3.3.1a) is exact, provided $u, v\in\mathbb{P}_n$. Using this fact, we define the map $\mathcal{I}_N : L^2(\mathbb{R})\to\mathbb{P}_n$,

$$\mathcal{I}_n[u] = \tfrac{\ell}{\pi}\sum_{k=0}^{n}\breve{u}_k\phi_k, \quad \breve{u}_k = \langle u, \phi_k\rangle_n.$$

We note that $\mathcal{I}_n$ is the identity in $\mathbb{P}_n$, as $\breve{u}_k = \hat{u}_k$ for such functions. In addition, from identities (3.1.1) it follows that

$$\mathcal{I}_n[u](x_j) = u(x_j), \quad 0\le j\le n, \tag{3.3.2}$$

provided u is well defined at the quadrature nodes. By virtue of the last identity, we view $\mathcal{I}_n[\cdot]$ as a Lagrange interpolation operator. Below, we establish several basic approximation properties of $\mathcal{I}_n$ that are pertinent for the numerical analysis of problem (1.0.1).

To begin, we show that the interpolation operator $\mathcal{I}_n$ is bounded as a map from $H^\alpha(\mathbb{R})$ to $L^2(\mathbb{R})$, provided $\alpha > \frac{1}{2}$.

Lemma 3.3.1 (Stability estimate)**.** *Assume $\alpha > \frac{1}{2}$, then*

$$\|\mathcal{I}_n\|_{H^\alpha(\mathbb{R})\to L^2(\mathbb{R})} \leq c\big(\tfrac{\ell\pi n}{2}\big)^{\frac{1}{2}}, \tag{3.3.3}$$

where the generic constant $c > 0$ does not depend on n.

Proof. By the classical Sobolev embedding theorem [3], we have $\|u\|_{L^\infty(\mathbb{R})} \leq c_\alpha \|u\|_{H^\alpha(\mathbb{R})}$, provided $\alpha > \frac{1}{2}$. Therefore, taking into account the accuracy of the quadrature (3.3.1) and the interpolation identity (3.3.2), we obtain

$$\begin{aligned}\|\mathcal{I}_n[u]\|^2_{L^2(\mathbb{R})} &= \tfrac{\pi}{2\ell(n+1)} \sum_{j=0}^{n} (\ell^2 + 4x_j^2)|u(x_j)|^2 \\ &\leq c_\alpha \Big[\tfrac{\pi}{2\ell(n+1)} \sum_{j=0}^{n} (\ell^2 + 4x_j^2)\Big] \|u\|^2_{H^\alpha(\mathbb{R})} =: c_\alpha C_n^2 \|u\|^2_{H^\alpha(\mathbb{R})}.\end{aligned}$$

The quantity C_n can be computed explicitly. From formula (3.3.1b) it follows that

$$C_n^2 = \tfrac{\pi\ell}{2(n+1)} \sum_{j=0}^{n} \tfrac{1}{\sin^2\theta_j} = \tfrac{\pi\ell}{2(n+1)} \sum_{j=0}^{n} U_n^2(t_j), \quad t_j = \cos\tfrac{2j+1}{2(n+1)}\pi,$$

where $U_n(t)$ is the Chebyshev polynomial of the second kind and the summation is interpreted as the $n+1$-nodes Gauss-Chebyshev quadrature associated with weight $w(x) = (1-x^2)^{-\frac{1}{2}}$. Using basic properties of the Gaussian quadratures, we infer

$$C_n^2 = \tfrac{\ell}{2} \int_{-1}^{1} U_n^2(t) \tfrac{dt}{\sqrt{1-t^2}}.$$

In view of the identity $U_n(t) = tU_{n-1}(t)+T_n(t)$ and the three-term recurrence formulas for $T_n(x)$ and $U_n(x)$ (see e.g. [2]), we obtain initially that

$$C_n^2 = 2C_{n-1}^2 - C_{n-2}^2, \quad n \geq 2, \quad C_0^2 = \tfrac{\pi\ell}{2}, \quad C_1 = \pi\ell$$

and then $C_n^2 = \frac{\pi\ell}{2}(n+1)$, for all $n \geq 0$. Hence, (3.3.3) follows. □

We note that $\mathbb{P}_n$ is a finite dimensional vector space. As a consequence, all norms in $\mathbb{P}_n$ are equivalent. In what follows, we need an estimate on the equivalence constant connecting $L^2(\mathbb{R})$ and $H^\alpha(\mathbb{R})$ norms.

Lemma 3.3.2 (The inverse inequality)**.** *Assume $u \in \mathbb{P}_n$ and $\alpha \in \mathbb{R}_+$, then*

$$\|u\|_{H^\alpha(\mathbb{R})} \leq c_\alpha (\tfrac{n}{2})^\alpha \|u\|_{L^2(\mathbb{R})}, \tag{3.3.4}$$

where the generic constant $c_\alpha > 0$ depends on $\alpha > 0$ and is uniformly bounded in $n > 0$.

Proof. (a) To begin, we let $\alpha = 1$ and, without loss of generality, assume $n = 2p+1$, $p \in \mathbb{N}_+$ and $u \in \mathbb{P}_n$. By virtue of (3.1.3a) and (3.1.3b), the action of the operator $\frac{d}{dx}$ on elements of $\mathbb{P}_n$ is given by

$$\begin{aligned}\tfrac{d}{dx}u = \tfrac{\ell}{\pi}\sum_{k=0}^{p+1} \phi_{2k+1}[\tfrac{k}{\ell}\hat{u}_{2k+2} - \tfrac{2k+1}{\ell}\hat{u}_{2k} + \tfrac{k+1}{\ell}\hat{u}_{2k+2}] \\ - \tfrac{\ell}{\pi}\sum_{k=0}^{p+1} \phi_{2k}[\tfrac{k}{\ell}\hat{u}_{2k-1} - \tfrac{2k+1}{\ell}\hat{u}_{2k+1} + \tfrac{k+1}{\ell}\hat{u}_{2k+3}],\end{aligned}$$

where $\hat{u}_k = 0$, whenever $k < 0$ or $k > n$. The latter formula indicates in particular that $\frac{d}{dx} : \mathbb{P}_n \to \mathbb{P}_{n+2}$.

Since $u \in \mathbb{P}_n$ is uniquely determined by its spectral coefficients, the space $\mathbb{P}_n$, equipped with the $L^2(\mathbb{R})$ norm is isometrically isomorphic to $\mathbb{R}^{n+1}$, equipped with the scaled Euclidean norm $|\cdot|^2 = \frac{\ell}{\pi}\sum_{k=0}^n |\cdot_k|^2$. In terms

of the spectral coefficients, the action of $\frac{d}{dx}$ is a linear transformation with block-tridiagonal matrix $\mathcal{D} \in \mathbb{R}^{(n+3)\times(n+1)}$, i.e.

$$\mathcal{D} = \mathcal{D}_{-1} + \mathcal{D}_0 + \mathcal{D}_1,$$

where the matrices $\mathcal{D}_{-1}$, $\mathcal{D}_0$ and $\mathcal{D}_1$ are made up of two-by-two square blocks in the lower, main and upper block-diagonals respectively. The diagonal and off-diagonal blocks are given respectively by

$$D_{ii} = \begin{bmatrix} 0 & \frac{2i+1}{\ell} \\ -\frac{2i+1}{\ell} & 0 \end{bmatrix}, \quad D_{i,i+1} = D_{i+1,i} = \begin{bmatrix} 0 & -\frac{i}{\ell} \\ \frac{i}{\ell} & 0 \end{bmatrix}.$$

Now let $\hat{u} \in \mathbb{R}^{n+1}$ be the vector of spectral coefficients, associated with $u \in \mathbb{P}_n$. Then

$$\begin{aligned} \|u\|^2_{H^1(\mathbb{R})} &= \|u\|^2_{L^2(\mathbb{R})} + \|u_x\|^2_{L^2(\mathbb{R})} = |\hat{u}|^2 + |\mathcal{D}\hat{u}|^2 \\ &\leq (1 + |\mathcal{D}|^2)|\hat{u}|^2 = (1 + |\mathcal{D}|^2)\|u\|^2_{L^2(\mathbb{R})}, \end{aligned}$$

where the subordinate norm $|\mathcal{D}|$ of matrix $\mathcal{D}$ is given by the formula

$$|\mathcal{D}| = \sup_{|\hat{u}|=1} |\mathcal{D}\hat{u}| = \sigma(\mathcal{D}^T\mathcal{D})^{\frac{1}{2}}$$

and $\sigma(\cdot)$ denotes the spectral radius of a matrix. It is easy to verify that $|\mathcal{D}_0| = \frac{2p+1}{\ell}$, $|\mathcal{D}_{-1}| = \frac{p+1}{\ell}$ and $|\mathcal{D}_1| = \frac{p}{\ell}$, so that

$$|\mathcal{D}| \leq |\mathcal{D}_{-1}| + |\mathcal{D}_0| + |\mathcal{D}_1| \leq \tfrac{2n}{\ell}.$$

The above calculations show that (3.3.4) holds when $\alpha = 1$.

(b) Consider $\mathcal{J} : \mathbb{P}_n \to H^\alpha(\mathbb{R})$, $\alpha > 0$, the natural embedding operator. From part (a) of the proof we have

$$\|\mathcal{J}u\|_{L^2(\mathbb{R})} \leq \|u\|_{L^2(\mathbb{R})}, \quad \|\mathcal{J}u\|_{H^1(\mathbb{R})} \leq c(\tfrac{n}{\ell})\|u\|_{L^2(\mathbb{R})}.$$

Since $H^\alpha(\mathbb{R}) = [L^2(\mathbb{R}), H^1(\mathbb{R})]_\alpha$, where $[\cdot,\cdot]_\alpha, \alpha \in (0,1)$ is the complex interpolation functor (see [6]), we conclude that $\mathcal{J} : L^2(\mathbb{R}) \to H^\alpha(\mathbb{R})$ is bounded and

$$\|\mathcal{J}\|_{L^2(\mathbb{R})\to H^\alpha(\mathbb{R})} \le \|\mathcal{J}\|^{1-\alpha}_{L^2(\mathbb{R})\to L^2(\mathbb{R})}\|\mathcal{J}\|^{\alpha}_{L^2(\mathbb{R})\to H^1(\mathbb{R})}.$$

Hence, (3.3.4) holds for $\alpha \in [0,1]$. For $\alpha > 1$ the result is obtained by iterating arguments, presented in parts (a) and (b) of the proof. □

Lemma 3.3.3. *Assume $\gamma > \frac{1}{2}$ and $\beta > 2\max\{\alpha,\gamma\}$, then*

$$\|(\mathcal{I} - \mathcal{I}_n)[u]\|_{H^\alpha(\mathbb{R})} \le c\big(\tfrac{n}{2}\big)^{\alpha+\frac{1}{2}+\gamma-\frac{\beta}{2}}\|u\|_{H^\beta_\beta(\mathbb{R})}, \tag{3.3.5}$$

where the constant $c > 0$ does not depend on u and/or $n > 0$.

Proof. Using the triangle inequality, combined with the inverse inequality (3.3.4), we obtain

$$\begin{aligned}\|(\mathcal{I}_n - \mathcal{I})[u]\|_{H^\alpha(\mathbb{R})} &\le \|\mathcal{I}_n(\mathcal{I} - \mathcal{P}_n)[u]\|_{H^\alpha} + \|(\mathcal{I} - \mathcal{P}_n)[u]\|_{H^\alpha(\mathbb{R})}\\ &\le c\big(\tfrac{n}{2}\big)^{\alpha}\|\mathcal{I}_n(\mathcal{I} - \mathcal{P}_n)[u]\|_{L^2(\mathbb{R})} + \|(\mathcal{I} - \mathcal{P}_n)[u]\|_{H^\alpha(\mathbb{R})}.\end{aligned}$$

Since $\mathcal{I}_n(\mathcal{I} - \mathcal{P}_n)[u] \in \mathbb{P}_n$, we apply Lemma 3.3.1 to obtain the bound

$$\|\mathcal{I}_n(\mathcal{I} - \mathcal{P}_n)[u]\|_{L^2(\mathbb{R})} \le c\big(\tfrac{n}{2}\big)^{\frac{1}{2}}\|(\mathcal{I} - \mathcal{P}_n)[u]\|_{H^\gamma(\mathbb{R})},$$

which holds for any $\gamma > \frac{1}{2}$. Hence, (3.3.5) follows from Lemma 3.2.1. □

Chapter 4

The fractional Schrödinger equation

In this Chapter, we briefly discuss the wellposedness of the nonlinear fractional Schrödinger equation (1.0.1). We follow the standard framework. First, we prove existsence of local classical solutions the result is then extended globally via explicit use of first integrals.

4.1 Local existence

Consider

$$iu_t = \beta D^{2\alpha} u + \nu |u|^{2p} u, \quad x \in \mathbb{R}, \quad t \in \mathbb{R}_+, \quad u(0) = u_0, \tag{4.1.1}$$

where $D^{2\alpha}$ is the pseudo-differential operator, associated with the Fourier symbol $|\xi|^{2\alpha}$, $0 < \alpha < 1$ and $p > 0$. To begin, we employ the standard Picard-Lindelöf iterations to show that (4.1.1) is locally solvable.

Theorem 4.1.1. *Assume $u_0 \in H^{2\alpha+\delta}(\mathbb{R})$, $\delta \geq 0$, then (4.1.1) has a unique local classical solution $u \in C([0,T], H^{2\alpha+\delta}(\mathbb{R})) \cap C^{(1)}((0,T), H^{\delta}(\mathbb{R}))$.*

Proof. (a) In our analysis it is convenient to work with Fourier images $\hat{u} = \mathcal{F}[u]$. Any classical solution $u \in C([0,T], H^{2\alpha+\delta}(\mathbb{R})) \cap C^{(1)}([0,T], H^{\delta}(\mathbb{R}))$ of (4.1.1), satisfies

$$\hat{u}(t) = \hat{u}_0 e^{-i\beta|\xi|^{2\alpha}t} + \nu \int_0^t e^{i\beta|\xi|^{2\alpha}(t-s)} \mathcal{F}[|u|^{2p}u](s)ds. \tag{4.1.2}$$

We show that for any input data $u_0 \in H^{2\alpha+\delta}(\mathbb{R})$, the integral equation (4.1.2) is uniquely solvable.

For a given $u_0 \in H^{2\alpha+\delta}(\mathbb{R})$, we let $\hat{v}(t) = e^{-i\beta|\xi|^{2\alpha}t}\hat{u}_0$ and define

$$\widehat{\mathcal{M}}(\hat{u}) = \hat{v}(t) + \nu \int_0^t e^{i\beta|\xi|^{2\alpha}(t-s)} \mathcal{F}[|u|^{2p}u](s)ds. \tag{4.1.3}$$

It is easy to verify that the nonlinear map $\mathcal{M}(u) := \mathcal{F}\big[\widehat{\mathcal{M}}(\hat{u})\big] : C([0,T], H^{2\alpha+\delta}(\mathbb{R})) \to C([0,T], H^{2\alpha+\delta}(\mathbb{R}))$ is bounded. Indeed, since $H^{2\alpha+\delta}(\mathbb{R})$, with $\alpha > \frac{1-2\delta}{4}$ is a Banach algebra, we have

$$\begin{aligned}
\|\mathcal{M}(u)\|_{C([0,T],H^{2\alpha+\delta})} &\le \|v\|_{C([0,T],H^{2\alpha+\delta})} + T|\nu|\big\||u|^{2p}u\big\|_{C([0,T],H^{2\alpha+\delta})} \\
&\le \|u_0\|_{H^{2\alpha+\delta}} + c_{2\alpha+\delta}T|\nu|\big\|u\big\|^{2p+1}_{C([0,T],H^{2\alpha+\delta})},
\end{aligned}$$

where $c_{2\alpha+\delta} > 0$, depends on the regularity parameter $2\alpha+\delta$ only.

(b) Assume $0 < r < 1$. The operator $\mathcal{M}$ maps the ball

$$B(v,r) = \{u \,|\, \|u - v\|_{C([0,T],H^{2\alpha+\delta})} < r\}$$

into itself, provided $T > 0$ is small. Indeed,

$$\begin{aligned}
\|\mathcal{M}(u) - v\|_{C([0,T],H^{2\alpha+\delta})} &\le T|\nu|c_{2\alpha+\delta}\|u\|^{2p+1}_{C([0,T],H^{2\alpha+\delta})} \\
&\le T|\nu|c_{2\alpha+\delta}\big(\|v\|_{C([0,T],H^{2\alpha+\delta})} + r\big)^{2p+1} \\
&< T|\nu|c_{2\alpha+\delta}\big(\|u_0\|_{H^{2\alpha+\delta}} + 1\big)^{2p+1} \le r,
\end{aligned}$$

provided

$$T \le \frac{r}{4(2p+1)|\nu|c_{2\alpha+\delta}\big(\|u_0\|_{H^{2\alpha+\delta}} + 1\big)^{2p+1}}. \tag{4.1.4}$$

(c) In fact $\mathcal{M}(u)$ is a contraction in $B(v,r)$, whenever T satisfies (4.1.4). Indeed, using the elementary inequality

$$\big||u|^{2p}u - |v|^{2p}v\big| \le (2p+1)|u-v|(|u|^{2p}+|v|^{2p}),$$

for any $u, w \in B(v,r) \subset C([0,T], H^{2\alpha+\delta}(\mathbb{R}))$ we obtain,

$$\begin{aligned}
&\|\mathcal{M}(u) - \mathcal{M}(w)\|_{C([0,T],H^{2\alpha+\delta})} \\
&\qquad \le T|\nu|\||u|^{2p}u - |w|^{2p}w\|_{C([0,T],H^{2\alpha+\delta})} \\
&\qquad \le T(2p+1)c_{2\alpha+\delta}|\nu|\big(\|u\|^{2p}_{C([0,T],H^{2\alpha+\delta})} \\
&\qquad + \|w\|^{2p}_{C([0,T],H^{2\alpha+\delta})}\big)\|u-w\|_{C([0,T],H^{2\alpha+\delta})} \\
&\qquad =: L\|u-w\|_{C([0,T],H^{2\alpha+\delta})}.
\end{aligned}$$

From the inclusion $u, w \in B(v,r)$ it follows also

$$\begin{aligned}
&\max\{\|u\|_{C([0,T],H^{2\alpha+\delta})}, \|w\|_{C([0,T],H^{2\alpha+\delta})}\} \\
&\qquad \le \|v\|_{C([0,T],H^{2\alpha+\delta})} + r \le \|u_0\|_{H^{2\alpha+\delta}} + 1.
\end{aligned}$$

Consequently,

$$L < T2(2p+1)c_{2\alpha+\delta}|\nu|(\|u_0\|_{H^{2\alpha+\delta}}+1)^{2p} < 1,$$

on account of (4.1.4).

(d) In view of parts (b)-(c) of the proof, the classical Banach fixed point theorem yields a unique mild solution $u \in C([0,T], H^{2\alpha+\delta}(\mathbb{R}))$ to the integral equation (4.1.2). The solution is classical for the right-hand side of (4.1.2) is differentiable with respect to t and belongs to $C([0,T], H^{\delta}(\mathbb{R}))$. □

4.2 Global solutions

In fact the local solution obtained in Theorem 4.1.1 can be extended globally to the real line. To show this, we observe that problem (4.1.1) has two formal

first integrals:

$$\mathcal{I}[u] = \tfrac{1}{2}\int_{\mathbb{R}} |u|^2 dx, \tag{4.2.1a}$$

$$\mathcal{H}[u] = \tfrac{1}{2}\int_{\mathbb{R}} \Big[\beta |D^\alpha u|^2 + \tfrac{\nu}{p+1}|u|^{2(p+1)}\Big] dx. \tag{4.2.1b}$$

Further, we have

Lemma 4.2.1. *Assume $u \in H^\alpha(\mathbb{R})$ and $\frac{1}{2} < \gamma \le \alpha$. Then, for any positive integer power $p > 0$, we have*

$$\|u^p\|_{H^\alpha(\mathbb{R})} \le c \|D^\alpha u\|_{L^2(\mathbb{R})} \|u\|^{p-1}_{H^\gamma(\mathbb{R})}, \tag{4.2.2}$$

where $c > 0$ does not depend on u.

Proof. In terms of Fourier images, we have

$$\begin{aligned}
\big|\mathcal{F}\big[D^\alpha u^p\big](\xi)\big| &\le |\xi|^\alpha |\hat{u}|^{*p}(\xi) \\
&= \int_{\mathbb{R}^{p-1}} \prod_{i=1}^{p-1} |\hat{u}(\xi_i)| \Big|\hat{u}\Big(\xi - \sum_{i=1}^{p-1}\xi_i\Big)\Big| \Big|\xi - \sum_{i=1}^{p-1}\xi_i + \sum_{i=1}^{p-1}\xi_i\Big|^\alpha d\xi_1 \dots d\xi_{p-1} \\
&\le C \int_{\mathbb{R}^{p-1}} \prod_{i=1}^{p-1} |\hat{u}(\xi_i)| \Big|\hat{u}\Big(\xi - \sum_{i=1}^{p-1}\xi_i\Big)\Big| \Big(\Big|\xi - \sum_{i=1}^{p-1}\xi_i\Big|^\alpha + \sum_{i=1}^{p-1}|\xi_i|^\alpha\Big) d\xi_1 \dots d\xi_{p-1} \\
&= pC \int_{\mathbb{R}^{p-1}} \prod_{i=1}^{p-1} |\hat{u}(\xi_i)| \Big|\hat{u}\Big(\xi - \sum_{i=1}^{p-1}\xi_i\Big)\Big| \Big|\xi - \sum_{i=1}^{p-1}\xi_i\Big|^\alpha d\xi_1 \dots d\xi_{p-1} \\
&= pC\big[|\hat{u}|^{*(p-1)} * |\xi^\alpha \hat{u}|\big](\xi),
\end{aligned}$$

where the positive constant C depends on α and p only and the symbol $*$ denotes the Fourier convolution product/power. Using the last inequality, combined with the integral version of Minkowski inequality, for $\gamma > \frac{1}{2}$ we obtain

$$\begin{aligned}
\|D^\alpha u^p\|_{L^2(\mathbb{R})} &\le pC \\
&\Big[\int_{\mathbb{R}} d\xi \Big[\int_{\mathbb{R}^{p-1}} \prod_{i=1}^{p-1} |\hat{u}(\xi_i)| \Big|\hat{u}\Big(\xi - \sum_{i=1}^{p-1}\xi_i\Big)\Big| \Big|\xi - \sum_{i=1}^{p-1}\xi_i\Big|^\alpha d\xi_1 \dots d\xi_{p-1}\Big]^2\Big]^{\frac{1}{2}} \\
&\le pC \|D^\alpha u\|_{L^2(\mathbb{R})} \|\hat{u}\|^{p-1}_{L^1(\mathbb{R})} \le c \|D^\alpha u\|_{L^2(\mathbb{R})} \|u\|^{p-1}_{H^\gamma(\mathbb{R})},
\end{aligned}$$

where $c > 0$ depends on γ and p only. $\square$

Lemma 4.2.1, combined with identities (4.2.1), yields the following a priori estimates:

Lemma 4.2.2. *Assume either $\beta\nu > 0$ and $\frac{p}{2(p+1)} \leq \alpha < 1$; or $\beta\nu < 0$ and $\frac{p}{2} < \alpha < 1$. Then the local classical solutions obtained in Theorem 4.1.1 satisfy*

$$\|u\|_{C([0,T],L^2(\mathbb{R}))} = \|u_0\|_{L^2(\mathbb{R})}, \tag{4.2.3a}$$

$$\|u\|_{C([0,T],H^\alpha(\mathbb{R}))} \leq C(u_0), \tag{4.2.3b}$$

$$\|u\|_{C([0,T],L^{2(p+1)}(\mathbb{R}))} \leq C(u_0), \tag{4.2.3c}$$

with $C(u_0) > 0$ that depends on $H^\alpha(\mathbb{R})$ norm of the initial data u_0 only.

Proof. (a) Since $\mathcal{I}[u]$ is preserved along the trajectories of (4.1.1), we conclude that (4.2.3a) is satisfied. Further, using the Gagliardo-Nirenberg inequality with index $\frac{p}{2(p+1)} \leq s \leq \alpha$, for $\mathcal{H}[u_0]$ we obtain the bound

$$\begin{aligned} |\mathcal{H}[u_0]| &\leq \tfrac{|\beta|}{2}\|D^\alpha u_0\|^2_{L^2(\mathbb{R})} + \tfrac{|\nu|}{2(p+1)}\|u_0\|^{2(p+1)}_{L^{2(p+1)}(\mathbb{R})} \\ &\leq \tfrac{|\beta|}{2}\|u_0\|^2_{H^\alpha(\mathbb{R})} + \tfrac{c|\nu|}{2(p+1)}\|u_0\|^{\frac{p}{s}}_{H^s(\mathbb{R})}\|u_0\|^{2(p+1)-\frac{p}{s}}_{L^2(\mathbb{R})} := C(u_0), \end{aligned} \tag{4.2.4}$$

where $c > 0$ is an absolute constant. Formula (4.2.4) indicates that the total energy of the system at initial time $t = 0$ is completely controlled by $H^\alpha(\mathbb{R})$ norm of the initial data.

(b) Assume initially that $\beta\nu > 0$. Since the Hamiltonian $\mathcal{H}[u]$ is conserved, we have

$$\tfrac{|\beta|}{2}\|D^\alpha u\|^2_{L^2(\mathbb{R})} + \tfrac{|\eta|}{2(p+1)}\|u\|_{L^{2(p+1)}(\mathbb{R})} = |\mathcal{H}[u_0]|.$$

The estimate, combined with bound (4.2.4) implies (4.2.3b) and (4.2.3c).

(c) In the case when $\beta\nu < 0$, we employ the Gagliardo-Nirenberg inequality with index $\frac{p}{2(p+1)} \leq \alpha$ to obtain

$$\begin{aligned} |\mathcal{H}[u_0]| &\geq \tfrac{|\beta|}{2}\|D^\alpha u\|^2_{L^2(\mathbb{R})} - \tfrac{|\eta|}{2(p+1)}\|u\|^{2(p+1)}_{L^{2(p+1)}(\mathbb{R})} \\ &\geq \tfrac{|\beta|}{2}\|D^\alpha u\|^2_{L^2(\mathbb{R})} - \tfrac{|\eta|}{2(p+1)}\|u\|^{\frac{p}{\alpha}}_{H^\alpha(\mathbb{R})}\|u\|^{2(p+1)-\frac{p}{\alpha}}_{L^2(\mathbb{R})}. \end{aligned}$$

The last inequality, combined with (4.2.3a), indicates that (4.2.3b) and (4.2.3c) are satisfied, provided $\beta\nu < 0$ and $\alpha > \frac{p}{2}$. □

With the aid of Lemmas 4.2.1 and 4.2.2, we obtain

Theorem 4.2.3. *Under the assumptions of Lemma 4.2.2, the classical solutions $u \in C([0,T], H^{2\alpha+\delta}(\mathbb{R})) \cap C^{(1)}((0,T), H^\delta(\mathbb{R}))$, $\delta \geq 0$, obtained in Theorem 4.1.1, are global in time.*

Proof. Using the variation of constants formula (4.1.2) and Lemma 4.2.1, we have

$$\begin{aligned} \|u\|_{H^{2\alpha+\delta}(\mathbb{R})}(t) &\leq \|u_0\|_{H^{2\alpha+\delta}(\mathbb{R})} + \int_0^t \||u|^{2p}u\|_{H^{2\alpha+\delta}(\mathbb{R})}(\tau)d\tau \\ &\leq \|u_0\|_{H^{2\alpha+\delta}(\mathbb{R})} + c\int_0^t \|u\|_{H^{2\alpha+\delta}(\mathbb{R})}(\tau)\|u\|^{2p}_{H^\gamma(\mathbb{R})}(\tau)d\tau, \end{aligned}$$

where $\frac{1}{2} < \gamma \leq 2\alpha$ is arbitrary. Let $\gamma = \alpha$, then,

$$\|u\|_{H^{2\alpha+\delta}(\mathbb{R})}(t) \leq C_1 + C_2\int_0^t \|u\|_{H^{2\alpha+\delta}(\mathbb{R})}(\tau)d\tau,$$

where, in view of Lemma 4.2.2, C_1 and C_2 are positive constants that depend on the initial data u_0 only. It follows from Gronwall's inequality that

$$\|u\|_{H^{2\alpha+\delta}(\mathbb{R})}(t) \leq \|u_0\|^{2\alpha+\delta}e^{C_2 t},$$

where $C_2 > 0$ depends on $\|u_0\|_{H^{\alpha+\delta}(\mathbb{R})}$ only. The last inequality indicates that local solutions, obtained in Theorem 4.1.1, cannot blow up in a finite time in the metric of $H^{2\alpha+\delta}(\mathbb{R})$ and hence are globally defined. □

Chapter 5

Christov-type spectral scheme for the fractional nonlinear Schrödinger equation

To begin, we rewrite (1.0.1) in the weak form:
Find $u \in C([0,T], H^{\alpha}(\mathbb{R})) \cap C^{(1)}((0,T), H^{-\alpha}(\mathbb{R}))$ such that

$$\langle iu_t, \phi\rangle = \beta\langle D^{\alpha}u, D^{\alpha}\phi\rangle + \nu\langle |u|^{2p}u, \phi\rangle, \tag{5.0.1a}$$

$$\langle u(0), \phi\rangle = \langle u_0, \phi\rangle, \tag{5.0.1b}$$

holds for all $\phi \in H^{\alpha}(\mathbb{R})$. To solve (5.0.1) the problem numerically, we employ Christov-type pseudospectral scheme. That is, we approximate the exact solution u by $u_n \in \mathbb{P}_n$, so that

$$\langle iu_{nt}, \phi\rangle = \beta\langle D^{\alpha}u_n, D^{\alpha}\phi\rangle + \nu\langle \mathcal{I}_n[|u_n|^{2p}u_n], \phi\rangle, \tag{5.0.2a}$$

$$\langle u(0), \phi\rangle = \langle \mathcal{I}_n[u_0], \phi\rangle, \tag{5.0.2b}$$

holds for all $\phi \in \mathbb{P}_n$. Problem (5.0.2) is equivalent to a system of ordinary differential equations that can be integrated in time using suitable time-stepping algorithms. Our main goal here is to show that the semi-discrete

scheme is stable, consistent and converges to the exact solutions of (5.0.1) as the discretization parameter n increases.

5.1 Stability

To begin, we observe that the semidiscretization (5.0.2) is Hamiltonian. Indeed, we have

$$\begin{aligned}
&\beta\langle D^\alpha u_n, D^\alpha\phi\rangle + \nu\langle \mathcal{I}_n[|u_n|^{2p}u_n], \phi\rangle \\
&= \beta\langle D^\alpha u_n, D^\alpha\phi\rangle + \nu\sum_{j=0}^{n} w_j|u_n|^{2p}(x_j)u_n(x_j)\phi(x_j) \\
&= \langle \nabla\mathcal{H}_n(u_n), \phi\rangle,
\end{aligned}$$

where

$$\begin{aligned}
\mathcal{H}_n(u_n) &= \tfrac{\beta}{2}\int_{\mathbb{R}} |D^\alpha u_n|^2 dx + \tfrac{\nu}{2(p+1)}\sum_{j=0}^{n} w_j|u_n|^{2(p+1)}(x_j) \\
&= \tfrac{1}{2}\int_{\mathbb{R}}\Big[\beta|D^\alpha u_n|^2 + \tfrac{\nu}{p+1}\mathcal{I}_n[|u_n|^{2p}]\mathcal{I}_n[|u_n|]^2\Big]dx.
\end{aligned}$$

Consequently, (5.0.2) is equivalent to

$$u_{nt} = -i\nabla\mathcal{H}_n(u_n), \quad u_n(0) = \mathcal{I}_n[u_0] = u_{n0}. \tag{5.1.1}$$

We employ this fact to show that the numerical solutions generated by (5.0.2) are uniformly bounded in $H^\alpha(\mathbb{R})$ as the discretization parameter $n \geq 0$ increases.

Lemma 5.1.1. *Assume $\alpha > \frac{1}{2}$ and either $\beta\nu > 0$ or $\beta\nu < 0$ and $\alpha > \frac{p}{2}$. Then*

$$\|u_n\|_{C(\mathbb{R},H^\alpha)} \leq c(\|u_{n0}\|_{H^\alpha}), \tag{5.1.2}$$

where $c(\cdot)$ is a positive bounded function of its argument which does not depend on $n > 0$.

Proof. First, we note that $\mathcal{I}(u_n) = \|\cdot\|_{L^2(\mathbb{R})}$ is preserved along the numerical trajectories u_n. Further, the hamiltonicity of (5.0.2) implies that $\mathcal{H}_n(u_n) = \mathcal{H}_n(u_{n0})$, for all $t \in \mathbb{R}$. Now if $\beta\nu > 0$, it follows that

$$\|u_n\|^2_{H^\alpha(\mathbb{R})} \leq \|u_{n0}\|^2 + \tfrac{2}{|\beta|}|\mathcal{H}_n(u_{n0})|,$$

for all $t \in \mathbb{R}$. In the case $\beta\nu < 0$, as in Lemma 4.2.2 we make use of the Gagliardo-Nirenberg inequality and classical Sobolev embeddings to obtain

$$\begin{aligned}
|\mathcal{H}_n(u_{n0})| &\geq \tfrac{|\beta|}{2}\|D^\alpha u_n\|^2_{L^2(\mathbb{R})} - \tfrac{|\nu|}{2(p+1)}\sum_{j=0}^{n} w_j |u_n|^{2p}(x_j)|u_n|^2(x_j) \\
&\geq \tfrac{|\beta|}{2}\|D^\alpha u_n\|^2_{L^2(\mathbb{R})} - \tfrac{|\nu|}{2(p+1)}\|u_n\|^2_{L^2(\mathbb{R})}\|u_n\|^{2p}_{L^\infty(\mathbb{R})} \\
&\geq \tfrac{|\beta|}{2}\|D^\alpha u_n\|^2_{L^2(\mathbb{R})} - \tfrac{c|\nu|}{2(p+1)}\|D^\alpha u_n\|^{\frac{p}{\alpha}}_{L^2(\mathbb{R})}\|u_n\|^{2(p+1)-\frac{p}{\alpha}}_{L^2(\mathbb{R})},
\end{aligned}$$

where $c > 0$ is a constant that does not depend on u_n or $n > 0$. Using Young's inequality, it is not difficult to verify that $\|D^\alpha u_n\|^2_{L^2(\mathbb{R})}$ is uniformly bounded in terms of the initial data u_{n0}, for all $t \in \mathbb{R}$, provided $\alpha > \frac{p}{2}$. □

The following result shows that the numerical scheme (5.0.2) is continuous with repsect to the input data, i.e. stable.

Lemma 5.1.2 (Stability)**.** *Consider the following two initial value problems: Find $u^i_n \in \mathbb{P}_n$, $i = 1, 2$, so that*

$$\langle iu^i_{nt}, \phi\rangle = \beta\langle D^\alpha u^i_n, D^\alpha\phi\rangle + \nu\langle \mathcal{I}_n[|u^i_n|^{2p}u^i_n], \phi\rangle + \langle f^i, \phi\rangle, \tag{5.1.3a}$$

$$u^i(0) = u^i_{n0}, \tag{5.1.3b}$$

holds for all $\phi \in \mathbb{P}_n$. If u^i_n, $i = 1, 2$, satisfy the estimate (5.1.2) *of Lemma 5.1.1, then*

$$\|u^1_n - u^2_n\|_{C([0,T],L^2(\mathbb{R}))} \leq c\big[\|u^1_{n0} - u^2_{n0}\|_{L^2(\mathbb{R})} + \|f^1 - f^2\|_{L^2([0,T]\times\mathbb{R})}\big], \tag{5.1.3c}$$

where the constant $c > 0$ depends on $\|u^i_{n0}\|_{H^\alpha(\mathbb{R})}$, $i = 1, 2$ and the terminal time $T > 0$ only.

Proof. Let $e_n = u_n^1 - u_n^2$, then from (5.1.3) it follows that

$$\begin{aligned}\langle ie_{nt}, \phi\rangle &= \beta\langle D^\alpha e_n, D^\alpha\phi\rangle + \nu\langle \mathcal{I}_n[|u_n^1|^{2p}u_n^1 - |u_n^2|^{2p}u_n^2], \phi\rangle \\ &\quad + \langle f^1 - f^2, \phi\rangle, \quad e_n(0) = e_{n0}.\end{aligned}$$

We let $\phi = ie_n$ in the last identity to obtain the bound

$$\begin{aligned}\tfrac{1}{2}\tfrac{d}{dt}\|e_n\|_{L^2(\mathbb{R})}^2 &= \nu\langle \mathcal{I}_n[|u_n^1|^{2p}u_n^1 - |u_n^2|^{2p}u_n^2], ie_n\rangle + \langle f^1 - f^2, ie_n\rangle \\ &= 2\nu\,\mathrm{Re}\sum_{j=0}^{n} w_j[|u_n^1|^{2p}u_n^1 - |u_n^2|^{2p}u_n^2](x_j)\overline{ie_n(x_j)} + \langle f^1 - f^2, ie_n\rangle \\ &\le 2\nu\Big(\sum_{k=1}^{2p}\|u_n^2\|_{L^\infty(\mathbb{R})}^k\|u_n^1\|_{L^\infty(\mathbb{R})}^{2p-k}\Big)\|e_n\|_{L^2(\mathbb{R})}^2 + \tfrac{1}{2}\|e_n\|_{L^2(\mathbb{R})}^2 + \tfrac{1}{2}\|f^1 - f^2\|_{L^2(\mathbb{R})}^2 \\ &\le c\|e_n\|_{L^2(\mathbb{R})}^2 + \tfrac{1}{2}\|f^1 - f^2\|_{L^2(\mathbb{R})}^2,\end{aligned}$$

where, in view of our assumptions, the generic constant $c > 0$ is completely controlled by the quantities $\|u_{n0}^i\|_{H^\alpha(\mathbb{R})}$, $i = 1, 2$ only. Now from Gronwall's inequality, it follows that

$$\|e_n\|_{L^2(\mathbb{R})}^2 \le e^{tc}\|e_{n0}\|_{L^2(\mathbb{R})}^2 + \int_0^t e^{(t-s)c}\|f^1 - f^2\|_{L^2(\mathbb{R})}^2(s)ds.$$

Hence, (5.1.3c) holds. □

5.2 Consitency and convergence

Let u be the exact weak solution to (5.0.1a) and define $\bar{u} = \mathcal{P}_n[u]$. Then for any $\phi \in \mathbb{P}_n$ the following is true

$$\begin{aligned}\langle i\bar{u}_{nt}, \phi\rangle &= \beta\langle D^\alpha\bar{u}_n, D^\alpha\phi\rangle + \nu\langle \mathcal{I}_n[|\bar{u}_n|^{2p}\bar{u}_n], \phi\rangle \\ &\quad + \beta\langle D^\alpha(\mathcal{I} - \mathcal{P}_n)[u], D^\alpha\phi\rangle + \nu\langle |u|^{2p}u - \mathcal{I}_n[|\bar{u}_n|^{2p}\bar{u}_n], \phi\rangle, \quad (5.2.1a)\\ \bar{u}_n(0) &= \mathcal{P}_n[u](0). \quad (5.2.1b)\end{aligned}$$

To show that the numerical scheme is consistent, we demonstrate that the defect

$$\begin{aligned} E_n(u) &= \beta D^{2\alpha}(\mathcal{I}-\mathcal{P}_n)[u] + \nu(|u|^{2p}u - \mathcal{I}_n[|\bar{u}_n|^{2p}\bar{u}_n]) \\ &=: \beta E_n^1(u) + \nu E_n^2(u) \end{aligned}$$

is small, provided the exact solution is sufficiently regular.

Lemma 5.2.1. *Assume $u \in L^{2(2p+1)}([0,T], H^{\beta}_{\beta}(\mathbb{R})) \cap C([0,T], H^{\alpha}(\mathbb{R}))$, with $\alpha > \frac{1}{2}$ and $\beta > 4\alpha$. Then the numerical defect satisfies*

$$\|E_n(u)\|_{L^2([0,T]\times\mathbb{R})} \leq c\big(\tfrac{n}{2}\big)^{2\alpha-\frac{\beta}{2}}\Big[1+\|u\|^p_{C([0,T],H^{\alpha}(\mathbb{R}))}\Big]\|u\|^{2p+1}_{L^{2(2p+1)}([0,T],H^{\beta}_{\beta}(\mathbb{R}))}, \tag{5.2.2}$$

where $c > 0$ does not depend on $n > 0$ and/or u.

Proof. We estimate $E_n^1(u)$ and $E_n^2(u)$ separately. In view of Lemmas 3.2.1, we have

$$\|E_n^1(u)\|_{L^2(\mathbb{R})} \leq \|(\mathcal{I}-\mathcal{P}_n)[u]\|_{H^{2\alpha}(\mathbb{R})} \leq c\big(\tfrac{n}{2}\big)^{2\alpha-\frac{\beta}{2}}\|u\|_{H^{\beta}_{\beta}(\mathbb{R})}. \tag{5.2.3}$$

To estimate $E_n^2(u)$, we write

$$\begin{aligned} E_n^2(u) &= (|u|^{2p}u - \mathcal{I}_n[|u|^{2p}u]) + \mathcal{I}_n[|u|^{2p}u - |\bar{u}|^{2p}\bar{u}] \\ &=: E_n^{21}(u) + E_n^{22}(u). \end{aligned}$$

For $E_n^{22}(u)$, we proceed as in Lemma 5.1.2 to obtain

$$\begin{aligned} \|E_n^{22}(u)\|^2_{L^2(\mathbb{R})} &= \sum_{j=0}^{n} w_j ||u|^{2p}(x_j)u(x_j) - |\bar{u}|^{2p}(x_j)\bar{u}(x_j)|^2 \\ &\leq \Big(\sum_{k=1}^{2p}\|u\|^k_{L^{\infty}(\mathbb{R})}\|\bar{u}\|^{2p-k}_{L^{\infty}(\mathbb{R})}\Big)\|(\mathcal{I}_n-\mathcal{P}_n)[u]\|^2_{L^2(\mathbb{R})}. \end{aligned}$$

Consequently, by virtue of Lemma 3.2.1,

$$\|E_n^{22}(u)\|^2_{L^2(\mathbb{R})} \leq c\Big(\sum_{k=1}^{2p} \|u\|^k_{H^\alpha(\mathbb{R})}\big[\|u\|_{H^\alpha(\mathbb{R})} + (\tfrac{n}{2})^{\alpha-\frac{\beta}{2}}\|u\|_{H^\beta_\beta(\mathbb{R})}\big]^{2p-k}\Big)(\tfrac{n}{2})^{-\beta}\|u\|^2_{H^\beta_\beta(\mathbb{R})}$$
$$\leq c\big(\tfrac{n}{2}\big)^{-\beta}\big[\|u\|_{C([0,T],H^\alpha(\mathbb{R}))} + (\tfrac{n}{2})^{\alpha-\frac{\beta}{2}}\|u\|_{H^\beta_\beta(\mathbb{R})}\big]^{2p}\|u\|^2_{H^\beta_\beta(\mathbb{R})}.$$

To bound $E_n^{21}(u)$, we recall that by virtue of Lemma 2.5.2, $H^\beta_\beta(\mathbb{R})$, $\beta > \frac{1}{2}$ is a Banach algebra. Hence, direct use of Lemma 3.3.3, yields

$$\|E_n^{21}(u)\|_{L^2(\mathbb{R})} = \|(\mathcal{I} - \mathcal{I}_n)[|u|^{2p}u]\|_{L^2(\mathbb{R})} \leq c(\tfrac{n}{2})^{\frac{1+2\alpha-\beta}{2}}\|u\|^{2p+1}_{H^\beta_\beta(\mathbb{R})}.$$

Combining all our estimates, we obtain the result. □

Lemmas 5.1.2 and 5.2.1, yield the convergence.

Theorem 5.2.2. *Assume $u \in L^{2(2p+1)}([0,T], H^\beta_\beta(\mathbb{R}))\cap C([0,T], H^\alpha(\mathbb{R}))$, with $\alpha > \frac{1}{2}$ and $\beta > 4\alpha$. Then the numerical solution satisfies*

$$\begin{aligned}\|u - u_n\|_{C([0,T],L^2(\mathbb{R}))} &\leq c\big(\tfrac{n}{2}\big)^{\frac{1+2\alpha-\beta}{2}}\|u_0\|_{H^\beta_\beta(\mathbb{R})} \\ &+ c\big(\tfrac{n}{2}\big)^{\frac{4\alpha-\beta}{2}}\Big[1 + \|u\|^p_{C([0,T],H^\alpha(\mathbb{R}))}\Big]\|u\|^{2p+1}_{L^{2(2p+1)}([0,T],H^\beta_\beta(\mathbb{R}))},\end{aligned} \tag{5.2.4}$$

where $c > 0$ does not depend on $n > 0$ and/or u.

Chapter 6

Implementation and numerical simulations

In this Chapter, we discuss several technical issues that arise in connection with the numerical scheme (5.0.2). In particular, we describe an appropriate time-stepping algorithm and preconditioners to improve computational efficiency of (5.0.2). We conclude the Chapter with several simulations which demonstrates the accuracy and performance of our scheme applied to the fractional nonlinear Schrödinger equation with different settings for the model parameters.

6.1 Implementation

In our simulations, we let $n = 2r$, where r is a positive integer. Then, the spatial semi-discretisation (5.0.2) yields the system of ODEs:

$$i\dot{Y} = \beta D_{2\alpha} Y + \nu F(Y), \tag{6.1.1a}$$

$$Y(0) = Y_0, \tag{6.1.1b}$$

where $D_{2\alpha} \in \mathbb{R}^{2r\times 2r}$ is the discrete fractional differentiation matrix, $F(Y)$ denotes the non-linearity and the concrete form of Y depends on the representation of the numerical solution. The latter can be either a vector of the discrete spectral coefficients

$$Y = (\breve{u}_0, \dots, \breve{u}_{2(r-1)}; \breve{u}_1, \dots, \breve{u}_{2r-1})^T \in \mathbb{C}^{2r},$$

or the vector of physical values of u_n, computed at the collocation points x_j,

$$Y = \big(u_n(x_0), \dots, u_n(x_{2r-1})\big)^T \in \mathbb{C}^{2r}, \quad x_j = \tfrac{\ell}{2}\cot\big(\tfrac{2j+1}{4r}\pi\big), \quad 0 \le j \le 2r-1.$$

The concrete form of the discrete fractional derivative $D_{2\alpha}$ depends on the realization of Y. If Y is the vector of spectral coefficients, then $D_{2\alpha}$ is block diagonal and is given by

$$D_{2\alpha} = \operatorname{diag}\{D_{r,2\alpha}, D_{r,2\alpha}\},$$

where $D_{r,2\alpha} \in \mathbb{R}^{r\times r}$ and

$$(D_{r,2\alpha})_{ij} = \tfrac{\ell}{\pi}\langle \phi_{2i}, D^{2\alpha}\phi_{2j}\rangle, \quad 0 \le i,j \le r-1.$$

The non-linearity $F(Y)$ has a simple representation when Y is a vector of physical values of u_n:

$$F(Y) = \big(|u_n(x_0)|^{2p}u_n(x_0), \dots, |u_n(x_{2r-1})|^{2p}u_n(x_{2r-1})\big)^T.$$

Independently of the concrete realization of Y, when computing the vector fields of (6.1.1) the direct and inverse Christov-Fourier transform

$$\breve{u}_i = \tfrac{\pi}{4\ell r}\sum_{j=0}^{2r-1}(\ell^2 + 4x_j^2)\hat{u}_n(x_j)\phi_i(x_j), \tag{6.1.2a}$$

$$u_n(x_j) = \tfrac{\ell}{\pi}\sum_{i=0}^{2r-1}\breve{u}_i\phi_i(x_j). \tag{6.1.2b}$$

must be used. Due to the connection of the Christov and the trigonometric bases, each operation requires $\mathcal{O}(r\log r)$ floating point operations.

6.1.1 Time-stepping

To integrate the semi-discrete system (6.1.1) in time, we employ the splitting approach. We let

$$G_1(Y) = -i\beta D_{2\alpha} Y, \quad G_2(Y) = -i\nu F(Y), \quad G(Y) = G_1(Y) + G_2(Y)$$

and dentote the flow maps, associated with the vector fields G, G_1 and G_2, by Φ_t, Φ_t^1 and Φ_t^2, respectively. For small values of t, we approximate the exact flow Φ_t of (6.1.3) by means of the Lie-Trotter splitting formula:

$$\Phi_t \approx \Phi_{\frac{t}{2}}^1 \circ \Phi_t^2 \circ \Phi_{\frac{t}{2}}^1. \tag{6.1.3}$$

We note that the flow of Φ_t^2 can be computed explicitly. If vector Y_0 represents physical values of the initial data $u_n(0)$ at the collocation points, then

$$\Phi_t^2 Y_0 = \mathrm{diag}\big\{e^{-i\nu t|u_n(x_0,0)|^{2p}}, \ldots, e^{-i\nu t|u_n(x_{2r-1},0)|^{2p}}\big\} Y_0.$$

To compute Φ_t^1 we have to solve the system of linear ODEs

$$\begin{aligned} i\dot{Y} &= \beta D_{2\alpha} Y, \\ Y(0) &= Y_0. \end{aligned}$$

Since the matrix $D_{2\alpha}$ is dense in either physical or Fourier spaces, it is not easy to compute the matrix exponent $e^{-it\beta D_{2\alpha}}$ explicitly. To overcome this difficulty, we approximate the solution using the implicit mid-point rule

$$Y(t) \approx Y_0 + tG_1\Big[\tfrac{1}{2}(Y_0 + Y(t))\Big].$$

This gives us

$$\begin{aligned} \Phi_t^1 &\approx (I + i\tfrac{t\beta}{2} D_{2\alpha})^{-1}(I - i\tfrac{t\beta}{2} D_{2\alpha}) \\ &= 2(I + i\tfrac{t\beta}{2} D_{2\alpha})^{-1} - I_0 = \Psi_t^1. \end{aligned}$$

Combining all our calculations, to advance the solution of (6.1.1) by one time step of length τ, we employ the algorithm

$$Y_1 = \Psi^1_{\frac{\tau}{2}} \circ \Phi^2_\tau \circ \Psi^1_{\frac{\tau}{2}} Y_0 = \Psi_\tau Y_0. \tag{6.1.4}$$

Formula (6.1.4) gives an explicit, symmetric, symplectic method of classical order 2. The major drawback of (6.1.4) is its low order of convergence. In the settings of Theorem 5.2.2, after a single time-step of size τ, we have

$$\|u(\tau) - Y_1\|_{L^2(\mathbb{R})} = \mathcal{O}\big(\tau^3 + r^{\frac{2p-2\beta-1}{4}}\big),$$

which shows that for large values of n the small spatial discretization error $\mathcal{O}\big(r^{\frac{2p-2\beta-1}{4}}\big)$ is completely dominated by the large time integration error $\mathcal{O}(\tau^3)$.

To improve the accuracy of (6.1.4), we employ the idea of composition, see [17]. Instead of Ψ_τ, at each integration step we use

$$Y_1 = \Psi_{\gamma_m \tau} \circ \cdots \circ \Psi_{\gamma_1 \tau} Y_0 = \Psi^m_\tau Y_0. \tag{6.1.5}$$

An appropriate choice of unknown coefficients γ_i, $1 \le i \le m$, yields higher order time-stepping algorithms. In particular, with $m = 17$ and

$$\begin{aligned}
\gamma_1 =& \gamma_{17} = 0.13020248308889008087881763,\\
\gamma_2 =& \gamma_{16} = 0.56116298177510838456196441,\\
\gamma_3 =& \gamma_{15} = -0.38947496264484728640807860,\\
\gamma_4 =& \gamma_{14} = 0.15884190655515560089621075,\\
\gamma_5 =& \gamma_{13} = -0.39590389413323757733623154,\\
\gamma_6 =& \gamma_{12} = 0.18453964097831570709183254,\\
\gamma_7 =& \gamma_{11} = 0.25837438768632204729397911,\\
\gamma_8 =& \gamma_{10} = 0.29501172360931029887096624,\\
\gamma_9 =& -0.60550853383003451169892108,
\end{aligned}$$

we have a symplectic and symmetric time-stepping scheme of order 8, [17]. A single time step of (6.1.5) yields the error

$$\|u(\tau) - Y_1\|_{L^2(\mathbb{R})} = \mathcal{O}\big(\tau^9 + r^{\frac{2p-2\beta-1}{4}}\big)$$

and we can observe spectral convergence already for moderate values of time step $\tau > 0$.

6.1.2 Preconditioning of linear systems

According to (6.1.5), advancing the numerical solution by a single integration time step involves the solution of linear systems of the form

$$Y = (I + \tfrac{i\tau\beta}{2} D_{2\alpha})W. \tag{6.1.6}$$

The problem is that in the physical space the fractional differentiation matrix $D_{2\alpha}$ is dense, while in the frequency space $D_{2\alpha}$ is two-by-two block diagonal

$$D_{2\alpha} = \operatorname{diag}(D_{r,2\alpha}, D_{r,2\alpha}),$$

with dense blocks $D_{r,2\alpha} \in \mathbb{R}^{r\times r}$. As a consequence, solving (6.1.5) using general direct methods would require $\mathcal{O}(r^3)$ floating point operations and is prohibitively expensive for large values of r. Fortunately, the matrices $D_{r,\alpha} \in \mathbb{R}^{r\times r}$, $\alpha \in \mathbb{R}$, have a very particular structure.

Lemma 6.1.1. *The matrix $D_{r,\alpha}$, $\alpha \in \mathbb{R}$ can be factorized as follows*

$$D_{r,\alpha} = T_{r,\alpha}^T R_{r,\alpha} T_{r,\alpha}, \tag{6.1.7a}$$

where

$$R_{r,\alpha} = \tfrac{1}{\ell^\alpha} \operatorname{diag}\Big(\tfrac{\Gamma(1+\alpha)}{0!}, \ldots, \tfrac{\Gamma(r+\alpha)}{(r-1)!}\Big), \tag{6.1.7b}$$

$$(T_{r,\alpha})_{ij} = \begin{cases} \binom{j-i-1-\alpha}{j-i}, & 1 \le i \le j \le r, \\ 0, & \textit{otherwise.} \end{cases} \tag{6.1.7c}$$

Furthermore $\{T_{r,\alpha}\}_{\alpha\in\mathbb{R}}$ is an analytic group of upper triangular Toeplitz operators, i.e. $T_{r,\alpha} = e^{\alpha G_r}$, with the generator given explicitly by

$$(G_r)_{ij} = \begin{cases} \frac{1}{j-i}, & 1 \le i < j \le r, \\ 0, & \textit{otherwise.} \end{cases} \tag{6.1.7d}$$

Proof. By the definition of $D_{r,2\alpha}$, in the frequency space we have

$$
\begin{aligned}
(D_{r,2\alpha})_{ij} &= \tfrac{\ell}{\pi}\langle \phi_{2i}, D^{2\alpha}\phi_{2j}\rangle = \tfrac{\ell}{\pi}\langle \hat{\phi}_{2i}, \widehat{D^{2\alpha}\phi_{2j}}\rangle \\
&= \tfrac{\ell}{\pi}\int_{\mathbb{R}} \tfrac{\pi}{2}\varphi_i^{\ell,0}(\xi)|\xi|^{2\alpha}\varphi_j^{\ell,0}(\xi)d\xi = \tfrac{1}{\ell^{2\alpha}}\int_{\mathbb{R}_+} e^{-\xi}\mathcal{L}_i^{(0)}(\xi)\mathcal{L}_j^{(0)}(\xi)\xi^{2\alpha}d\xi \\
&= \tfrac{1}{\ell^{2\alpha}}\int_{\mathbb{R}_+} e^{-\xi}\Big[\sum_{m=0}^{i}\mathcal{L}_{i-m}^{(-1-2\alpha)}(0)\mathcal{L}_m^{(2\alpha)}(\xi)\Big]\Big[\sum_{k=0}^{j}\mathcal{L}_{j-k}^{(-1-2\alpha)}(0)\mathcal{L}_k^{(2\alpha)}(\xi)\Big]\xi^{2\alpha}d\xi \\
&= \tfrac{1}{\ell^{2\alpha}}\sum_{m=0}^{i}\mathcal{L}_{i-m}^{(-1-2\alpha)}(0)\sum_{k=0}^{j}\mathcal{L}_{j-k}^{(-1-2\alpha)}(0)\delta_{mk}\tfrac{\Gamma(m+2\alpha+1)}{\Gamma(m+1)} \\
&= \tfrac{1}{\ell^{2\alpha}}\sum_{m=0}^{\min\{i,j\}}\mathcal{L}_{i-m}^{(-1-2\alpha)}(0)\mathcal{L}_{j-m}^{(-1-2\alpha)}(0)\tfrac{\Gamma(m+2\alpha+1)}{\Gamma(m+1)} \\
&= \sum_{m=0}^{r}(T_{r,2\alpha})_{im}(R_{r,2\alpha})_{mm}(T_{r,2\alpha})_{jm},
\end{aligned}
$$

which is equivalent to (6.1.7a)-(6.1.7c), with α, replaced by 2α, as $\mathcal{L}_n^{(\alpha)}(0) = \binom{n-\alpha}{n}$, for any $n \geq 0$ and $\alpha \in \mathbb{C}$, see [2].

The group property

$$T_{r,\alpha}T_{r,\beta} = T_{r,\alpha+\beta}, \quad \alpha, \beta \in \mathbb{C},$$

follows directly from the identity

$$\sum_{i=0}^{n}\mathcal{L}_i^{(\alpha)}(x)\mathcal{L}_{n-i}^{(\beta)}(y) = \mathcal{L}_n^{(\alpha+\beta+1)}(x+y),$$

which holds for all $x, y, \alpha, \beta \in \mathbb{C}$, [2]. Formula (6.1.7d) is the consequence of the identity $G_r = \frac{d}{d\alpha}T_{r,\alpha}\Big|_{\alpha=0}$. □

From Lemma 6.1.1, it follows that the matrix of the linear system (6.1.6) can be written as a product of Toeplitz and diagonal matrices. Unfortunately, unlike purely Toeplitz coefficient matrices, there exist no fast direct algorithms for linear systems, whose matrix is a sum/product of diagonal and Toeplitz matrices and we have to resort to iterations. It is well known

that Krylov-subspace iteration schemes converge fast when the coefficient matrices are small rank perturbations of a matrix whose spectrum clusters at a single point [35]. Unfortunately, as seen from (6.1.7), for matrices $D_{r,2\alpha}$ this is not the case. The eigenvalues are real, positive and are scattered in the large interval $[\mathcal{O}(r^{-2\alpha}), \mathcal{O}(r^{2\alpha})]$.

To improve the situation, we are forced to use a preconditioner. In the context of fractional differentiation matrices it is customary to use circulant preconditioners, see [26, 27] and references therein. In our project, we adopt an alternative approach. Let

$$\mathcal{M}_\alpha(z) = \left(I + \tfrac{i\tau\beta}{2} T_{r,z}^T R_{r,2\alpha} T_{r,z}\right)^{-1}.$$

Lemma 6.1.1, implies that

(i) $\mathcal{M}_\alpha^{-1}(z) \in \mathbb{C}^{r\times r}$ are banded matrices, with bandwidth $2z+1$, for integer values of parameter z;

(ii) the standard subordinate Euclidean norms of $\mathcal{M}_\alpha(z)$, are bounded by 1, uniformly with respect to $z \in \mathbb{R}$ and $r \geq 1$;

(iii) $\mathcal{M}_\alpha(z)$ is an analytic matrix valued function of z in a small complex neighborhood of the real axis $\mathbb{R}$.

In view of properties (i)-(iii) above, we approximate $\mathcal{M}_\alpha(z)$ by a Hermite interpolation polynomial $P_\alpha^{2s-1}(z) \in \mathbb{C}^{r\times r}$, of degree $2s-1$ in z, which satisfies

$$\tfrac{d^j}{dz^j} P_\alpha^{2s-1}(z)\Big|_{z=1,2} = \tfrac{d^j}{dz^j} \mathcal{M}_\alpha(z)\big|_{z=1,2}, \quad 0 \leq j \leq s-1. \tag{6.1.8}$$

By properties (ii)-(iii), $P_\alpha^{2r-1}(2\alpha)$ approximates $\mathcal{M}_\alpha(2\alpha)$ and we can use $P_\alpha^{2s-1}(2\alpha)$ as a preconditioner, while in view of property (i) and (6.1.7d), computing the matrix-vector product $P_\alpha^{2s-1}(2\alpha)Y$ involves solving systems of linear equations with tri- and five-diagonal symmetric matrices multiplied,

when $s > 1$, by the group generator G_r and by its transpose G_r^T. We note that solving systems with banded matrices can be done at the cost of $\mathcal{O}(r)$ operations, while a matrix-vector multiplication by triangular Toeplitz matrices G_r and G_r^T can be accomplished in $\mathcal{O}(r \log r)$ flops via FFT. Hence, the total computational cost of preconditioning in a Krylov-type iteration schemes is $\mathcal{O}(r)$ for $s = 1$ and $\mathcal{O}(r \log r)$ for $s \geq 2$, which is better than (if $s = 1$) or comparable to (if $s \geq 2$) the standard circulant preconditioners described in the literature [26, 27].

The complete theoretical analysis of the preconditioner $P_\alpha^{2s-1}(z)$ falls outside the scope of this dissertation. As a partial substitute, Fig. 6.1 contains the spectrum distributions of the operator $P_\alpha^{2s-1}(2\alpha)\mathcal{M}_{2\alpha}^{-1}(2\alpha) - I$, for $r = 2^4, 2^6, 2^8$ and $s = 1, 2, 3, 4, 5$, with $\beta = 1$, $\tau = \frac{1}{2}$ and $\alpha \in \left[\frac{1}{2}, 1\right]$. The calculations show that for all values of r and s and $\alpha \in \left[\frac{1}{2}, 1\right]$, the entire spectrum $\sigma(P_\alpha^{2s-1}(2\alpha)\mathcal{M}_{2\alpha}^{-1}(2\alpha))$ of the preconditioned operator $P_\alpha^{2s-1}(2\alpha)\mathcal{M}_{2\alpha}^{-1}(2\alpha)$ is contained in a small complex neighborhood of $\lambda = 1$, while the deviation

$$d_{r,s} = \sup_{\frac{1}{2} \leq \alpha \leq 1} \operatorname{dist}(\sigma(P_\alpha^{2s-1}(2\alpha)\mathcal{M}_{2\alpha}^{-1}(2\alpha)), \{1\}),$$

decreases as the order s of the preconditioner increases.

To show the effect of preconditioner $P_\alpha^{2s-1}(2\alpha)$ on the convergence rate of Krylov-type iterations, we consider (6.1.6), where vector Y is given by $\mathcal{I}_{2r}\left[\frac{1}{1+x^2}\right]$, $r = 2^i$, $4 \leq i \leq 10$. We let $\beta = 1$, $\tau = \frac{1}{2}$ and solve (6.1.6) using preconditioned GMRES scheme (see [35]) with no preconditioner $s = 0$ and with the preconditioner $P_\alpha^{2s-1}(2\alpha)$, $s = 1, 2, 3, 4, 5$. We stop iterations when either the numerical defect is less than 10^{-12}, or when the total number of iterations exceeds the value of 50.

The results of simulations for $\alpha = \frac{5}{8}, \frac{3}{4}, \frac{7}{8}$ are reported in Tables 6.1.1, 6.1.2 and 6.1.3, respectively. Each table is divided into a number of horizontal blocks, corresponding to a particular value of the parameter s. In each block,

Table 6.1.1: Preconditioned GMRES for problem (6.1.6), $\alpha = \frac{5}{8}$.

r	2^4	2^5	2^6	2^7	2^8	2^9	2^{10}
$s=0$	$1.578 \cdot 10^{-11}$	$4.069 \cdot 10^{-11}$	$1.137 \cdot 10^{-04}$	$2.008 \cdot 10^{-03}$	$7.228 \cdot 10^{-03}$	$9.427 \cdot 10^{-03}$	$1.848 \cdot 10^{-02}$
	$5.615 \cdot 10^{-03}$	$8.519 \cdot 10^{-03}$	$9.878 \cdot 10^{-03}$	$1.345 \cdot 10^{-02}$	$3.448 \cdot 10^{-02}$	$6.113 \cdot 10^{-02}$	$8.156 \cdot 10^{-02}$
	27	49	50	50	50	50	50
$s=1$	$5.693 \cdot 10^{-11}$	$4.786 \cdot 10^{-11}$	$4.786 \cdot 10^{-11}$	$4.786 \cdot 10^{-11}$	$4.786 \cdot 10^{-11}$	$4.787 \cdot 10^{-11}$	$4.788 \cdot 10^{-11}$
	$3.087 \cdot 10^{-03}$	$1.973 \cdot 10^{-03}$	$4.770 \cdot 10^{-03}$	$2.585 \cdot 10^{-03}$	$6.596 \cdot 10^{-03}$	$1.411 \cdot 10^{-02}$	$1.669 \cdot 10^{-02}$
	10	10	10	10	10	10	10
$s=2$	$6.173 \cdot 10^{-12}$	$5.443 \cdot 10^{-12}$	$5.443 \cdot 10^{-12}$	$5.444 \cdot 10^{-12}$	$5.454 \cdot 10^{-12}$	$5.500 \cdot 10^{-12}$	$5.543 \cdot 10^{-12}$
	$5.108 \cdot 10^{-03}$	$2.544 \cdot 10^{-03}$	$4.074 \cdot 10^{-03}$	$3.676 \cdot 10^{-03}$	$1.351 \cdot 10^{-02}$	$1.819 \cdot 10^{-02}$	$2.336 \cdot 10^{-02}$
	6	6	6	6	6	6	6
$s=3$	$1.829 \cdot 10^{-12}$	$1.719 \cdot 10^{-12}$	$1.719 \cdot 10^{-12}$	$1.720 \cdot 10^{-12}$	$1.731 \cdot 10^{-12}$	$1.837 \cdot 10^{-12}$	$2.040 \cdot 10^{-12}$
	$4.986 \cdot 10^{-03}$	$3.247 \cdot 10^{-03}$	$4.803 \cdot 10^{-03}$	$7.349 \cdot 10^{-03}$	$1.540 \cdot 10^{-02}$	$4.502 \cdot 10^{-02}$	$3.711 \cdot 10^{-02}$
	4	4	4	4	4	4	4
$s=4$	$4.684 \cdot 10^{-11}$	$4.638 \cdot 10^{-11}$	$4.638 \cdot 10^{-11}$	$4.638 \cdot 10^{-11}$	$4.642 \cdot 10^{-11}$	$4.655 \cdot 10^{-11}$	$4.668 \cdot 10^{-11}$
	$4.820 \cdot 10^{-03}$	$4.729 \cdot 10^{-03}$	$5.730 \cdot 10^{-03}$	$6.139 \cdot 10^{-03}$	$2.390 \cdot 10^{-02}$	$7.674 \cdot 10^{-02}$	$6.319 \cdot 10^{-02}$
	3	3	3	3	3	3	3
$s=5$	$4.869 \cdot 10^{-13}$	$4.732 \cdot 10^{-13}$	$4.732 \cdot 10^{-13}$	$4.741 \cdot 10^{-13}$	$5.526 \cdot 10^{-13}$	$1.278 \cdot 10^{-12}$	$2.692 \cdot 10^{-12}$
	$4.697 \cdot 10^{-03}$	$5.965 \cdot 10^{-03}$	$5.378 \cdot 10^{-03}$	$8.625 \cdot 10^{-03}$	$3.571 \cdot 10^{-02}$	$1.035 \cdot 10^{-01}$	$1.068 \cdot 10^{-01}$
	2	2	2	2	2	2	2

the first row contains actual numerical errors, the second the execution times in seconds and the last one the total number of the GMRES iterations.

As seen from all three tables, the preconditioning does improve the computational performance in terms of both accuracy and the speed of computations. Note however, as the value of s increases, the numerical error and number of iterations are getting smaller but the execution time is increases. This is connected with the fact that the computational complexity of a matrix vector multiplication $P_{\alpha}^{2s-1}(2\alpha)\mathcal{M}_{2\alpha}^{-1}(2\alpha)Y$ increases together with the preconditioner order s.

Table 6.1.2: Preconditioned GMRES for problem (6.1.6), $\alpha = \frac{3}{4}$.

r	2^4	2^5	2^6	2^7	2^8	2^9	2^{10}
$s=0$	$3.929 \cdot 10^{-11}$	$4.715 \cdot 10^{-10}$	$3.521 \cdot 10^{-03}$	$2.043 \cdot 10^{-02}$	$3.772 \cdot 10^{-02}$	$6.128 \cdot 10^{-02}$	$4.356 \cdot 10^{-02}$
	$7.094 \cdot 10^{-03}$	$1.997 \cdot 10^{-02}$	$1.579 \cdot 10^{-02}$	$1.930 \cdot 10^{-02}$	$4.966 \cdot 10^{-02}$	$8.389 \cdot 10^{-02}$	$8.629 \cdot 10^{-02}$
	27	50	50	50	50	50	50
$s=1$	$1.832 \cdot 10^{-11}$	$1.111 \cdot 10^{-11}$	$1.111 \cdot 10^{-11}$	$1.111 \cdot 10^{-11}$	$1.111 \cdot 10^{-11}$	$1.111 \cdot 10^{-11}$	$1.113 \cdot 10^{-11}$
	$3.463 \cdot 10^{-03}$	$3.940 \cdot 10^{-03}$	$3.943 \cdot 10^{-03}$	$3.987 \cdot 10^{-03}$	$1.558 \cdot 10^{-02}$	$1.775 \cdot 10^{-02}$	$2.230 \cdot 10^{-02}$
	12	12	12	12	12	12	12
$s=2$	$5.626 \cdot 10^{-11}$	$4.908 \cdot 10^{-11}$	$4.908 \cdot 10^{-11}$	$4.909 \cdot 10^{-11}$	$4.926 \cdot 10^{-11}$	$4.951 \cdot 10^{-11}$	$4.942 \cdot 10^{-11}$
	$4.200 \cdot 10^{-03}$	$5.349 \cdot 10^{-03}$	$5.908 \cdot 10^{-03}$	$3.907 \cdot 10^{-03}$	$1.746 \cdot 10^{-02}$	$1.981 \cdot 10^{-02}$	$2.424 \cdot 10^{-02}$
	6	6	6	6	6	6	6
$s=3$	$2.020 \cdot 10^{-11}$	$1.957 \cdot 10^{-11}$	$1.957 \cdot 10^{-11}$	$1.959 \cdot 10^{-11}$	$2.040 \cdot 10^{-11}$	$2.342 \cdot 10^{-11}$	$2.522 \cdot 10^{-11}$
	$5.689 \cdot 10^{-03}$	$7.222 \cdot 10^{-03}$	$6.030 \cdot 10^{-03}$	$6.935 \cdot 10^{-03}$	$2.229 \cdot 10^{-02}$	$3.992 \cdot 10^{-02}$	$4.010 \cdot 10^{-02}$
	4	4	4	4	4	4	4
$s=4$	$1.679 \cdot 10^{-14}$	$1.653 \cdot 10^{-14}$	$1.654 \cdot 10^{-14}$	$2.861 \cdot 10^{-14}$	$6.627 \cdot 10^{-13}$	$4.189 \cdot 10^{-12}$	$1.128 \cdot 10^{-11}$
	$8.018 \cdot 10^{-03}$	$9.756 \cdot 10^{-03}$	$1.024 \cdot 10^{-02}$	$8.429 \cdot 10^{-03}$	$4.561 \cdot 10^{-02}$	$8.587 \cdot 10^{-02}$	$8.429 \cdot 10^{-02}$
	4	4	4	4	4	4	4
$s=5$	$2.590 \cdot 10^{-12}$	$2.377 \cdot 10^{-12}$	$2.377 \cdot 10^{-12}$	$2.918 \cdot 10^{-12}$	$1.714 \cdot 10^{-11}$	$5.912 \cdot 10^{-11}$	$1.136 \cdot 10^{-11}$
	$6.888 \cdot 10^{-03}$	$1.101 \cdot 10^{-02}$	$6.859 \cdot 10^{-03}$	$9.707 \cdot 10^{-03}$	$6.473 \cdot 10^{-02}$	$1.037 \cdot 10^{-01}$	$1.316 \cdot 10^{-01}$
	2	2	2	2	2	2	3

Table 6.1.3: Preconditioned GMRES for problem (6.1.6), $\alpha = \frac{7}{8}$.

r	2^4	2^5	2^6	2^7	2^8	2^9	2^{10}
$s=0$	$5.961 \cdot 10^{-11}$	$4.211 \cdot 10^{-09}$	$2.529 \cdot 10^{-02}$	$7.298 \cdot 10^{-02}$	$1.191 \cdot 10^{-01}$	$1.119 \cdot 10^{-01}$	$1.586 \cdot 10^{-01}$
	$5.425 \cdot 10^{-03}$	$1.049 \cdot 10^{-02}$	$9.462 \cdot 10^{-03}$	$1.859 \cdot 10^{-02}$	$3.382 \cdot 10^{-02}$	$8.056 \cdot 10^{-02}$	$8.235 \cdot 10^{-02}$
	27	50	50	50	50	50	50
$s=1$	$7.391 \cdot 10^{-11}$	$5.975 \cdot 10^{-11}$	$5.975 \cdot 10^{-11}$	$5.975 \cdot 10^{-11}$	$5.975 \cdot 10^{-11}$	$5.975 \cdot 10^{-11}$	$5.975 \cdot 10^{-11}$
	$3.555 \cdot 10^{-03}$	$2.816 \cdot 10^{-03}$	$3.410 \cdot 10^{-03}$	$2.125 \cdot 10^{-03}$	$8.122 \cdot 10^{-03}$	$1.780 \cdot 10^{-02}$	$1.824 \cdot 10^{-02}$
	11	11	11	11	11	11	11
$s=2$	$5.030 \cdot 10^{-12}$	$4.398 \cdot 10^{-12}$	$4.398 \cdot 10^{-12}$	$4.400 \cdot 10^{-12}$	$4.408 \cdot 10^{-12}$	$4.408 \cdot 10^{-12}$	$4.403 \cdot 10^{-12}$
	$4.778 \cdot 10^{-03}$	$2.456 \cdot 10^{-03}$	$4.406 \cdot 10^{-03}$	$5.234 \cdot 10^{-03}$	$1.155 \cdot 10^{-02}$	$2.675 \cdot 10^{-02}$	$2.269 \cdot 10^{-02}$
	6	6	6	6	6	6	6
$s=3$	$1.233 \cdot 10^{-12}$	$1.222 \cdot 10^{-12}$	$1.222 \cdot 10^{-12}$	$1.227 \cdot 10^{-12}$	$1.334 \cdot 10^{-12}$	$1.546 \cdot 10^{-12}$	$1.618 \cdot 10^{-12}$
	$3.900 \cdot 10^{-03}$	$4.461 \cdot 10^{-03}$	$5.593 \cdot 10^{-03}$	$4.761 \cdot 10^{-03}$	$1.457 \cdot 10^{-02}$	$5.870 \cdot 10^{-02}$	$3.669 \cdot 10^{-02}$
	4	4	4	4	4	4	4
$s=4$	$4.498 \cdot 10^{-11}$	$4.462 \cdot 10^{-11}$	$4.462 \cdot 10^{-11}$	$4.475 \cdot 10^{-11}$	$4.595 \cdot 10^{-11}$	$4.783 \cdot 10^{-11}$	$4.826 \cdot 10^{-11}$
	$3.734 \cdot 10^{-03}$	$3.814 \cdot 10^{-03}$	$4.358 \cdot 10^{-03}$	$5.083 \cdot 10^{-03}$	$1.973 \cdot 10^{-02}$	$6.518 \cdot 10^{-02}$	$4.959 \cdot 10^{-02}$
	2	2	2	2	2	2	2
$s=5$	$5.049 \cdot 10^{-14}$	$4.401 \cdot 10^{-14}$	$4.421 \cdot 10^{-14}$	$2.170 \cdot 10^{-13}$	$1.892 \cdot 10^{-12}$	$5.695 \cdot 10^{-12}$	$9.780 \cdot 10^{-12}$
	$4.978 \cdot 10^{-03}$	$5.171 \cdot 10^{-03}$	$8.056 \cdot 10^{-03}$	$8.783 \cdot 10^{-03}$	$6.809 \cdot 10^{-02}$	$9.601 \cdot 10^{-02}$	$1.040 \cdot 10^{-01}$
	2	2	2	2	2	2	2

6.2 Simulations

In this section we demonstrate the efficiency of the numerical scheme (5.0.2) of Chapter 5, by applying it to the fractional nonlinear Schrödinger equation, with different values of the parameters α, β, ν and p.

6.2.1 Example 1

Apart from the special cases of $\alpha = \frac{1}{2}$ and $\alpha = 2$, the closed form solutions to equation (4.1.1) are unknown. To illustrate the computational accuracy of the numerical scheme (5.0.2), we augment the original model with a source term, so that the numerical solution is given explicitly by

$$u(x,t) = \frac{e^{i\gamma t}}{1+x^2}.$$

For simulations, we let $\beta = \nu = p = 1$ and integrate the resulting semidiscrete equation (6.1.1) numerically in time interval $[0, 2\pi]$, using the timestepping procedure (6.1.5). The results of simulations for several values of $r \in [2^4, 2^9]$ and $\alpha \in [\frac{1}{2}, 1]$ are shown in Fig. 6.2.

The two top diagrams contains the $L^\infty([0,T], L^2(\mathbb{R}))$ and $L^\infty([0,T] \times \mathbb{R})$ errors versus r and α. As seen from the diagrams both errors exhibit spectral convergence (the corresponding lines are concave) when $\alpha = \frac{1}{2}, 1$. This is expected, for in these two special cases the source term $f = iu_t - \beta D^{2\alpha}u - \nu|u|^{2p}u$ belongs to the space $H^\beta_\beta(\mathbb{R})$, for any $\beta > 0$ and, according to Theorem 5.2.2, the error decreases faster than any negative power of $r = \frac{n}{2}$.

The situation changes for fractional values of 2α. Direct calculations show that $D^{2\alpha}\frac{1}{1+x^2} \in H^\beta_\beta(\mathbb{R})$, provided $\beta < 4\alpha + 1$. As a consequence, combining Lemma 5.1.2 and Theorem 5.2.2, we conclude that the semidiscretization error behaves as $\mathcal{O}\big(n^{\varepsilon-2\alpha}\big)$, where $\varepsilon > 0$ is arbitrary small. Hence, we expect almost $\mathcal{O}(n^{-1})$ convergence rate for fractional values of 2α near 1. Further,

we expect the convergence rate to increases gradually to $\mathcal{O}(n^{-2})$, when 2α approaches 2. The theoretical observation is in a good agreement with the numerical results displayed in the top two diagrams of Fig. 6.2. One can clearly see that the slopes of the error curves decrease gradually as the parameter α increases.

To provide further insight into the typical error behavior, we plotted the pointwise errors obtained with $r = 2^6$ in the four bottom diagrams of Fig. 6.2. The numerical error for $\alpha = \frac{5}{8}, \frac{7}{8}$ are significantly larger than the errors at $\alpha = \frac{1}{2}, 1$. For fractional values of 2α near 2, the errors are smaller than the errors for 2α near 1.

6.2.2 Example 2

In our second experiment, we repeat the calculations of Example 1. However, this time, we adjust the source term so that the exact solution reads

$$u(x,t) = \frac{e^{i\gamma t}x}{1+x^2}.$$

The results of simulations, displayed in Fig 6.3, are qualitatively very similar to those, observed in Example 1. Indeed, the numerical scheme converges spectrally for $\alpha = \frac{1}{2}, 1$, while convergence rate is algebraic for fractional values of 2α. Similarly to Example 1, the algebraic convergence rate is almost $\mathcal{O}(n^{-1})$ for $\alpha \approx \frac{1}{2}$ and gradually increases to $\mathcal{O}(n^{-2})$ for $\alpha \approx 1$.

6.2.3 Example 3

As mentioned in Example 1, closed form solutions for the fractional Schrödinger equation (4.1.1) are readily available only in the case of $\alpha = 1$ and $p = 1$. In this settings problem (4.1.1) reduces to the classical cubic nonlinear

Schrödinger equation whose solutions can be recovered via the inverse scattering transform [1]. In particular, in the focusing case ($\beta = 1$, $\nu = -2$ in our formulation), the inverse scattering transform yields the so called J-soliton solutions, describing propagation and elastic collision of J traveling waves. The J-soliton shape is controlled by a number of real parameters, including amplitudes – a_j, velocities – v_j, centers – ξ_j and phases – ϕ_j, $1 \le j \le J$, and is given by the explicit formula [1]

$$u(x,t) = 2i\frac{\det G^c}{\det G},$$

where

$$k = \Big(\tfrac{v_j + ia_j}{2},\ 1 \le j \le J\Big), \quad K = \Big(\tfrac{1}{k_i - k_j^*},\ 1 \le i,j \le J\Big),$$
$$y = i\Big(a_j e^{a_j\xi_j + i(\phi_j + 2xk_j - 4tk_j^2)},\ 1 \le j \le J\Big),$$
$$G = I + K\,\mathrm{diag}(y^*)K^*\,\mathrm{diag}(y), \quad G^c = \begin{pmatrix} 0 & y^T \\ \mathbb{1} & G \end{pmatrix}.$$

In this example, we test the accuracy of the scheme (5.0.2) using the classical cubic nonlinear Schrödinger equation associated with $\beta = 1$, $\nu = -2$ and $\alpha = 1$. As an exact solution, we take a 2-soliton ($J = 2$), whose shape is controlled by $a_1 = 2$, $a_2 = 1$, $v_1 = -\frac{1}{2}$, $v_2 = \frac{1}{2}$, $\xi_1 = 2$, $\xi_2 = -\frac{1}{2}$ and $\phi_1 = \phi_2 = 0$. In this settings, the exact solution describes an elastic collision (at time $t = \frac{3}{4}$) of two traveling waves. We compare the dynamics of the exact and numerical solutions in time interval $[0, 2\pi]$.

The results of the simulations are summarized in the top diagram of Fig. 6.4. One can clearly see that the $L^2(\mathbb{R})$ and $L^\infty(\mathbb{R})$ errors (blue and green curves, respectively) decrease spectrally. This is expected as the $H^\beta_\beta(\mathbb{R})$ norm of the exact solution is finite for all values of $\beta > 0$. Further, in the absence of a source term, the continuous model (4.1.1) and the numerical scheme (6.1.1)

are both conservative. Hence, we expect good preservation of the discrete Hamiltonian $\mathcal{H}_n(\cdot)$ and the $L^2(\mathbb{R})$-norm along numerical trajectories. The red and the orange curves in the top diagram of Fig. 6.4, corresponding to the largest deviation in the Hamiltonian and in the $L^2(\mathbb{R})$-norm, indicate that this is indeed the case. Both quantities remain small independently of the size of the semidiscretization parameter r.

The results of Examples 1 and 2, as well as the top diagram of Fig 6.4, demonstrate that the numerical scheme (5.0.2) is reliable and allows to reproduce actual dynamics of exact solutions for any $\alpha \in [\frac{1}{2}, 1]$ quite accurately. Using this observation, we simulate the solutions to problem (4.1.1), for $\alpha = \frac{7}{8}, \frac{3}{4}$ in the time interval $[0, 2\pi]$. As the input data, we take the initial profile of the exact 2-soliton $u(x, 0)$, shown in the two bottom diagrams of Fig. 6.4. The numerical solution with $\alpha = \frac{7}{8}, \frac{3}{4}$, plotted in the four middle diagrams of Fig. 6.4 indicate that in the presence of fractional derivatives the collision of traveling waves is no longer elastic. Immediately after collision, the solutions develop high frequency small amplitude spurious waves moving away from the original traveling waves. Furthermore, one can see that the oscillation frequency of the spurious waves increases as α moves further away from the critical value of 1. Theoretically, this is connected to the decrease in the degree of the local smoothing effect induced by the linear hyperbolic propagator $\exp\{-i\beta D^{2\alpha}t\}$, see [34].

6.2.4 Example 4

In our final example, we repeat the calculations of Example 3, but this time for a 3–soliton. We let $J = 3$, $a_1 = 2$, $a_2 = 3$, $a_3 = 1$, $v_1 = \frac{1}{2}$, $v_2 = 0$, $v_3 = -\frac{1}{2}$, $\xi_1 = 0$, $\xi_2 = 2$, $\xi_3 = 5$ and $\phi_1 = \phi_2 = \phi_3 = 0$ and keep the remaining parameters unchanged. The results of the simulations are shown in

Fig 6.5 and are almost identical to that of Example 3. As before, the scheme (5.0.2) converges spectrally for $\alpha = 1$ (see the top diagram in Fig. 6.5), the semidiscrete first integrals $\mathcal{H}_n(\cdot)$ and $\|\cdot\|_{L^2(\mathbb{R})}$ are preserved with high accuracy, independently of the value of the semidiscretization parameter r. We cannot judge the simulation accuracy for $\alpha = \frac{3}{4}, \frac{7}{8}$, but the qualitative behaviour of the numerical solutions is the same as in Example 3. For fractional values of 2α, the traveling waves collisions are inelastic, each traveling wave give rise to a small amplitude oscillations whose frequencies increase as α decreases.

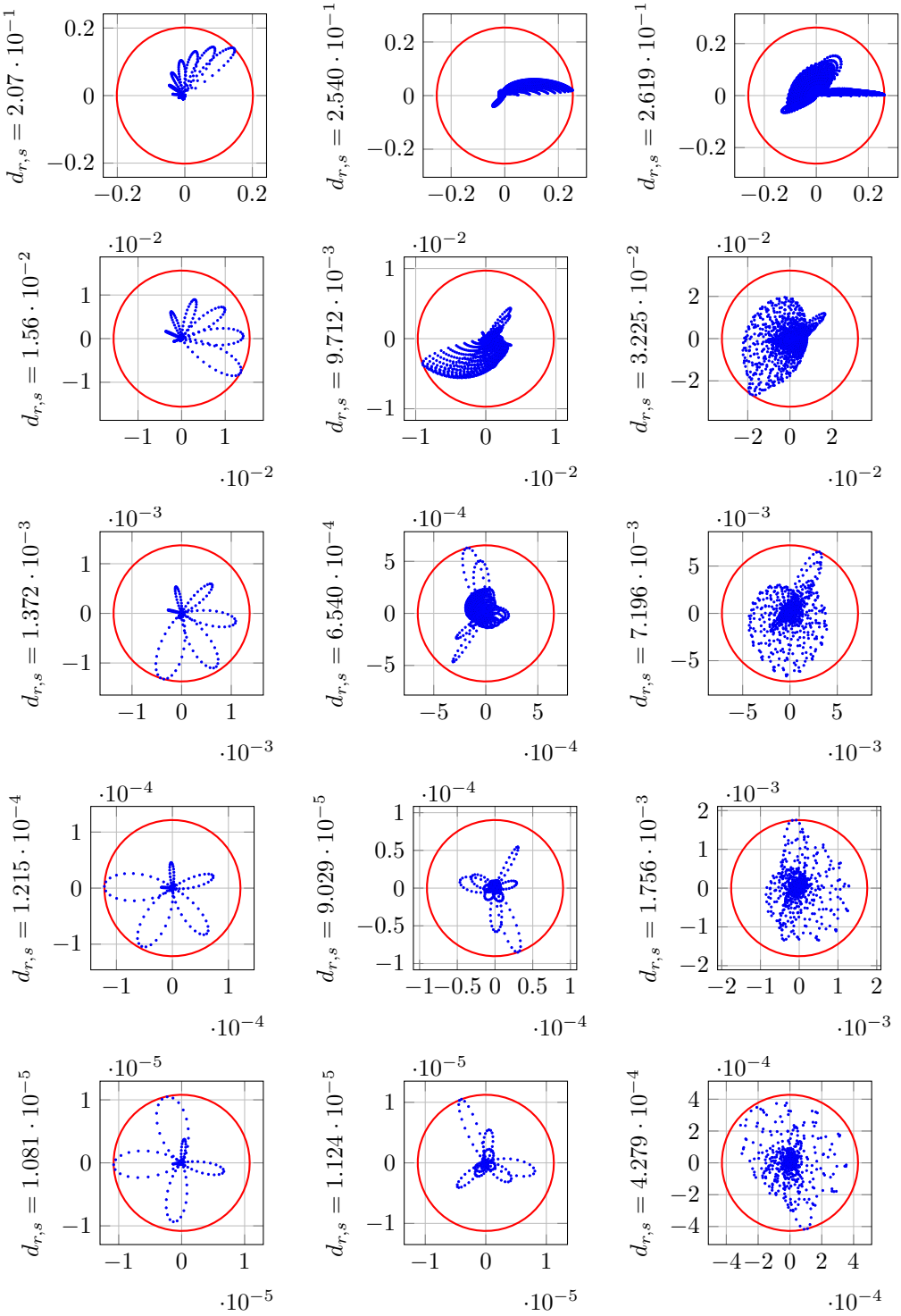

Figure 6.1: Eigenvalues of $P_\alpha^{2s-1}(2\alpha)\mathcal{M}_{2\alpha}^{-1}(2\alpha)$, $\alpha \in \left[\frac{1}{2}, 1\right]$, rows: $s = 1, 2, 3, 4, 5$, columns: $r = 2^4, 2^6, 2^8$.

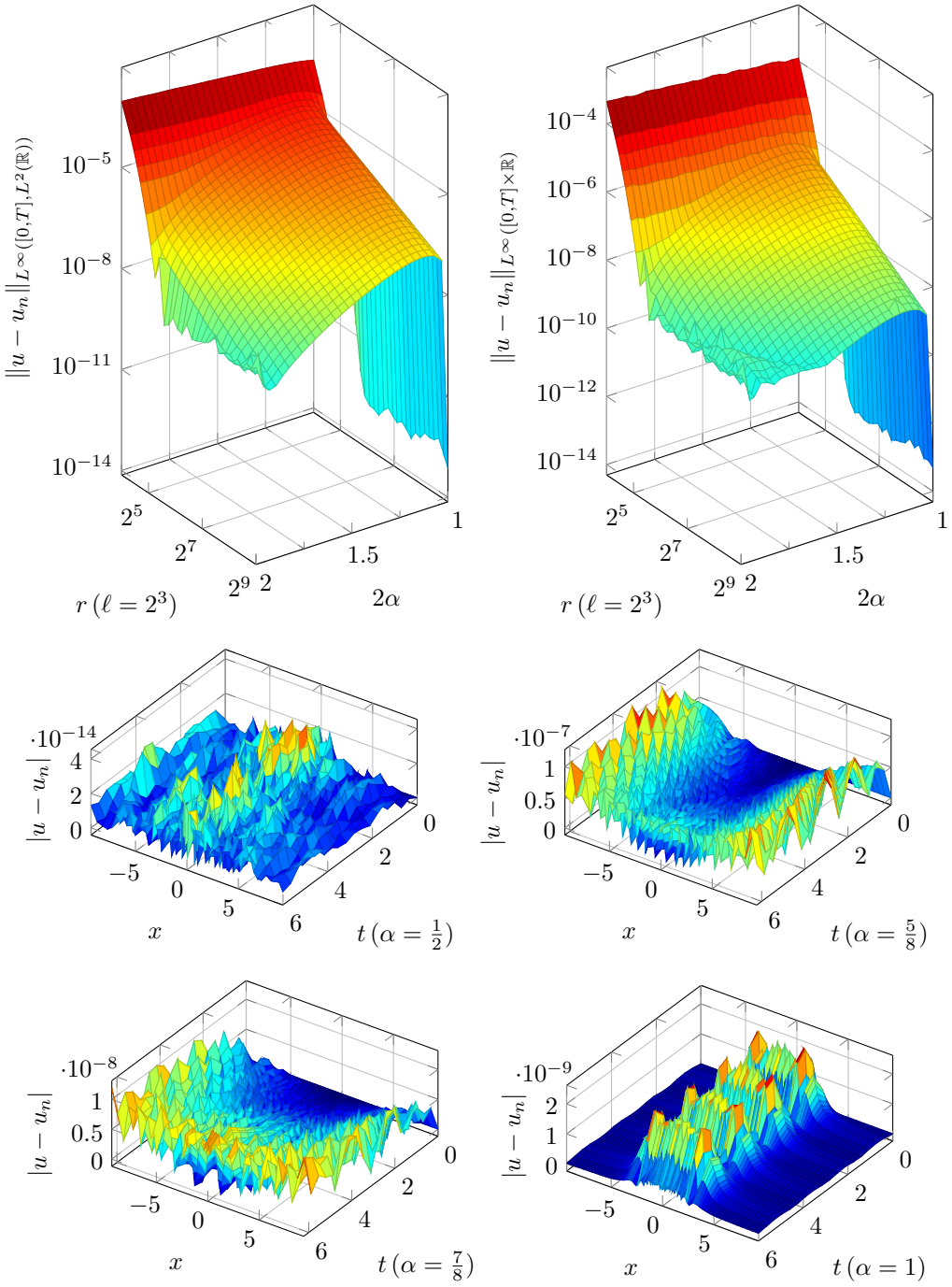

Figure 6.2: Example 1. The work precision diagrams, $2^4 \leq r \leq 2^8$, $\frac{1}{2} \leq \alpha \leq 1$, $t \in [0, 2\pi]$. The pointwise errors, $r = 2^6$, left-to-right and top-to-bottom $\alpha = \frac{1}{2}, \frac{5}{8}, \frac{7}{8}, 1$.

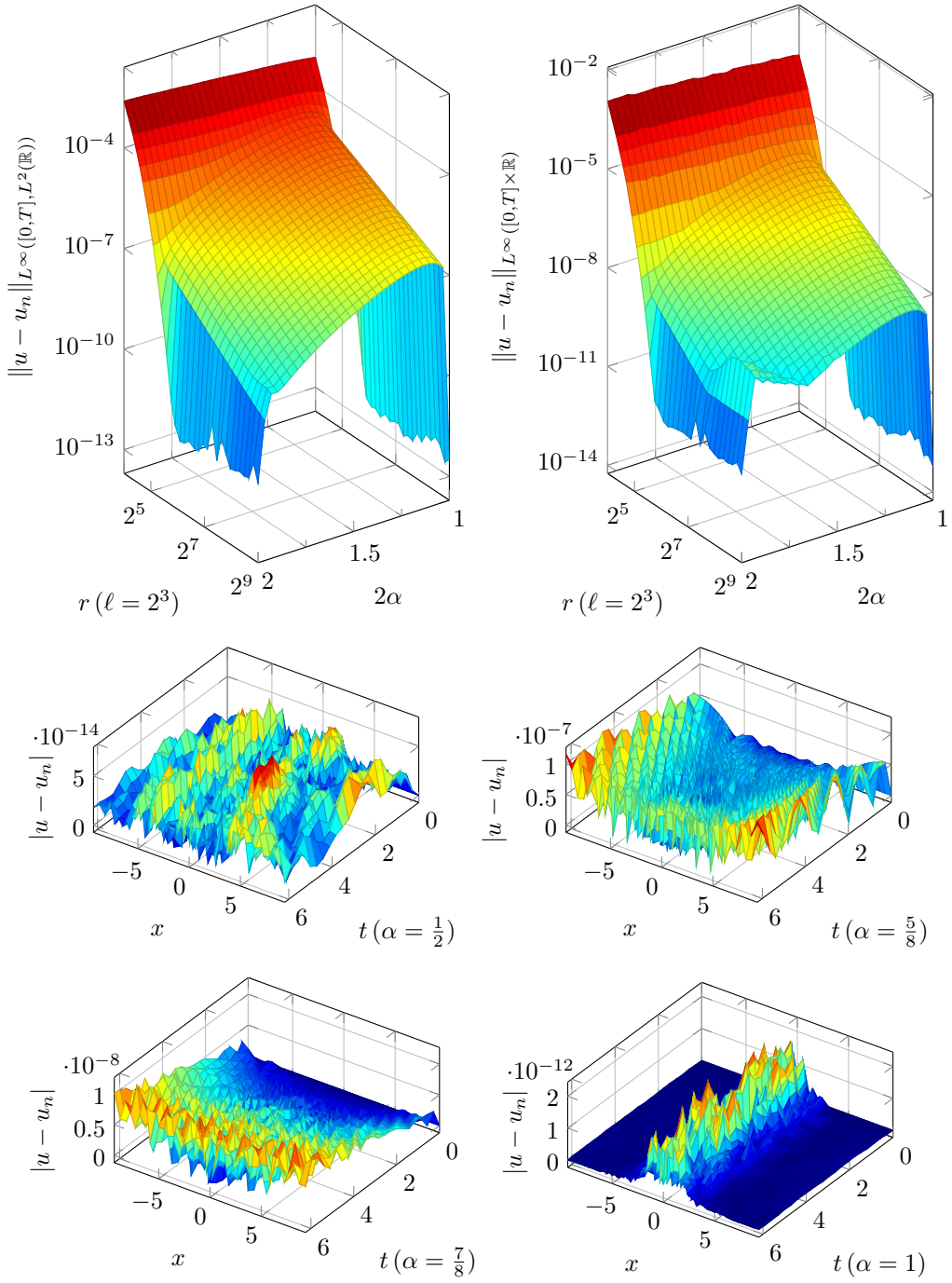

Figure 6.3: Example 2. The work precision diagrams, $2^4 \leq r \leq 2^8$, $\frac{1}{2} \leq \alpha \leq 1$, $t \in [0, 2\pi]$. The pointwise errors, $r = 2^6$, left-to-right and top-to-bottom $\alpha = \frac{1}{2}, \frac{5}{8}, \frac{7}{8}, 1$.

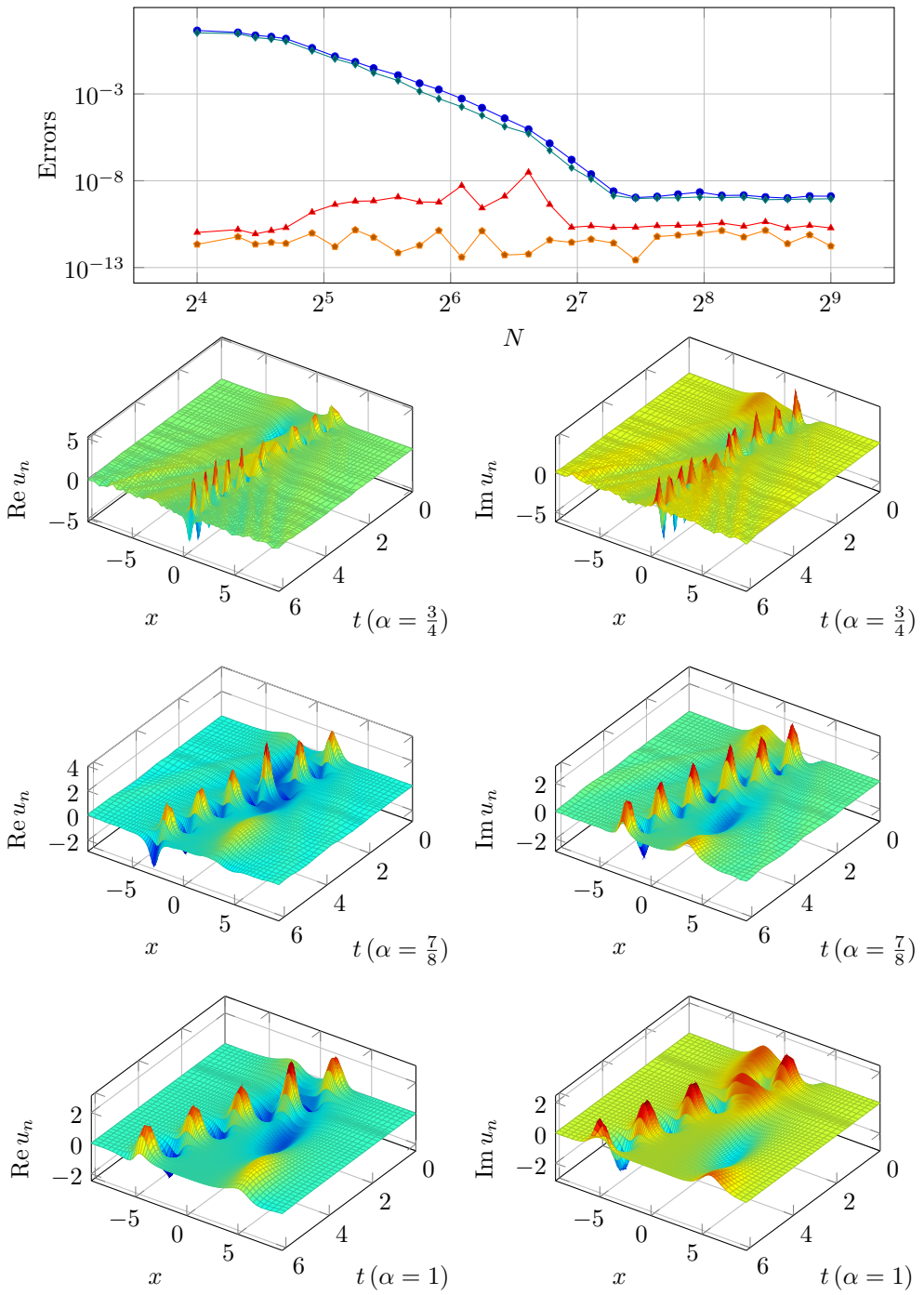

Figure 6.4: Example 3. The work precision diagram ($\alpha = 2$): $L^\infty([0,T], L^2(\mathbb{R}))$ (blue, circle) and $L^\infty([0,T] \times \mathbb{R})$ (green, diamond) errors; $\max_t |\mathcal{H}_n(u_n(t)) - \mathcal{H}_n(u_{n0})|$ (red, triangle); $\max_t |\|u_n(t)\|^2_{L^2(\mathbb{R})} - \|u_{n0}\|^2_{L^2(\mathbb{R})}|$ (orange, pentagon). The numerical solutions, $r = 2^6$, $\alpha = \frac{3}{4}, \frac{7}{8}, 1$.

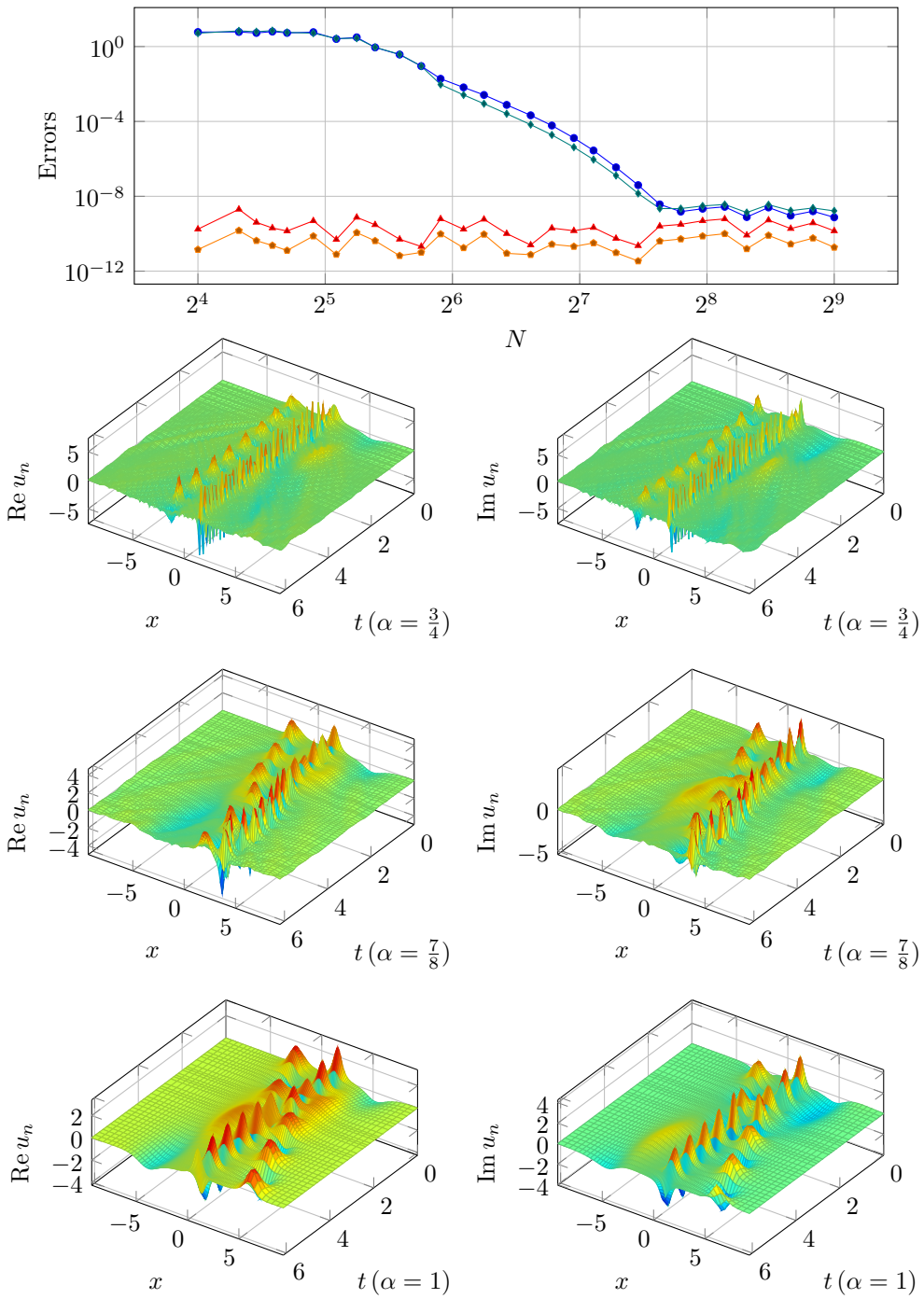

Figure 6.5: Example 4. The work precision diagram ($\alpha = 2$): $L^{\infty}([0,T], L^2(\mathbb{R}))$ (blue, circle) and $L^{\infty}([0,T] \times \mathbb{R})$ (green, diamond) errors; $\max_t |\mathcal{H}_n(u_n(t)) - \mathcal{H}_n(u_{n0})|$ (red, triangle); $\max_t |\|u_n(t)\|^2_{L^2(\mathbb{R})} - \|u_{n0}\|^2_{L^2(\mathbb{R})}|$ (orange, pentagon). The numerical solutions, $r = 2^6$, $\alpha = \frac{3}{4}, \frac{7}{8}, 1$.

Chapter 7

Conclusion

The fractional nonlinear Schrödinger equation appears in a number of plasma physics and in quantum mechanics applications and, apart from the classical case of $\alpha = 1$, has no closed form solutions and hence requires a rigorous numerical treatment. The latter, despite some progress, represents a significant challenge. Particularly in unbounded domains, where methods based on the domain truncation and/or use of transparent boundary conditions are either unavailable or do not work well for fractional values of 2α, while the only known global Hermite-type spectral scheme suffers from slow convergence.

To overcome these difficulties, in this dissertation we proposed to use Christov-type pseudospectral scheme and provided its rigorous stability and convergence analyses. Further, we presented a detailed discussion, related to the practical implementation of our numerical scheme. In particular, we described an appropriate high order explicit time-stepping algorithm that preserves the dynamical features (simplecticity) of the continuous model. We provided a detailed account on solving linear systems with a semidiscrete fractional Laplacian. We did demonstrate that an appropriate choice of a preconditioner requires very few Krylov-type iterations and yields an

$\mathcal{O}(r \log r)$-complexity computational algorithm suitable for large scale simulations. The theoretical conclusions as well as the practical computational efficiency of our scheme is confirmed by a series of concrete numerical experiments.

Bibliography

[1] M.J. Ablowitz, B. Prinari, and A.D. Trubatch. *Discrete and Continuous Nonlinear Schrödinger Systems*. Cambridge University Press, 2004.

[2] M. Abramowitz and I.A. Stegun. *Handbook of Mathematical Functions with Tables*. Dover, 1964.

[3] R.A. Adams and J.J.F. Fournier. *Sobolev Spaces*. Elsevier, 2nd edition, 2003.

[4] P. Amore, F.M. Fernandez, C.P. Hofmann, and R.A. Saenz. Collocation method for fractional quantum mechanics. *J. Math. Phys.*, 51:122101, 2010.

[5] J. Banasiak, N. Parumasur, W.D. Poka, and S. Shindin. Pseudospectral Laguerre approximation of transport-fragmentation equations. *Appl. Math. Comput.*, 239:107–125, 2014.

[6] J. Bergh and J. Löfström. *Interpolation Spaces: An Introduction*. Springer-Verlag, Berlin, Heidelberg, New-York, 1976.

[7] A.H. Bhrawy and M.A. Abdelkawy. A fully spectral collocation approximation for multi-dimensional fractional Schrödinger equations. *Journal of Computational Physics*, 294:462–483, 2015.

[8] J.P. Boyd. The orthogonal rational functions of Higgins and Christov and algebraically mapped Chebyshev polynomials. *J. Approx. Theory*, 61:98–105, 1990.

[9] J.P. Boyd. *Chebyshev and Fourier Spectral Methods*. Dover Publications, Inc., New York, 2000.

[10] C. Canuto, A. Quarteroni, M.Y. Hussani, and T.A. Zang. *Spectral Methods: Fundamental in Single Domains*. Springer-verlag. Berlin, Heidelberg, 2006.

[11] C.I. Christov. A complete orthonormal sysytem of functions in $L^2(-\infty, \infty)$ space. *SIAM J. Appl. Math.*, 42:1337–1344, 1982.

[12] S. Duo and Y. Zang. Mass-conservative Fourier spectral methods for solving the fractional nonlinear Schrödinger equation. *Computers and Mathematics with Applications*, 71:2257–2271, 2016.

[13] J. Fröhlich, B.L.G. Jonsson, and E. Lenzmann. Boson stars as solitary waves. *Comm. Math. Phys.*, 274:1–30, 2007.

[14] D. Funaro. *Polynomial Approximation of Differential Equations*. Springer Verlag, 1992.

[15] L. Grafakos. *Modern Fourier Analysis*. Springer, 2009.

[16] B. Guo and Z. Huo. Well-posedness for the nonlinear fractional Schrödinger equation and inviscid limit behavior of solution for the fractional Ginzburg-Landau equation. *Fractional Calc. Appl. Anal.*, 16:226–242, 2013.

[17] E. Hairer, C. Lubich, and G. Wanner. *Geometric Numerical Integration*. Springer, 2006.

[18] J. Hesthaven, S. Gottlieb, and D. Gottlieb. *Spectral Method for Time-Dependent Problems*. Cambridge University Press, Cambridge, UK, 2007.

[19] A. Iserles and M. Webb. A family of orthogonal rational functions and other orthogonal systems with a skew-Hermitian differentiation matrix. *Technical report, DAMTP, University of Cambridge.*, 2019.

[20] K. Kirkpatrick, E. Lenzmann, and G. Staffilani. On the continuum limit for discrete NLS with long-range lattice interactions. *Comm. Math. Phys.*, 317:563–591, 2013.

[21] C. Klein, C. Sparber, and P. Markowich. Numerical study of fractional nonlinear Schrödinger equations. *Proc. R. Soc. A*, 470:1–26, 2014.

[22] E. Lenzmann. Well-posedness for semi-relativistic Hartree equations of critical type. *Math. Phys. Anal. Geom.*, 10:43–64, 2007.

[23] F. Malmquist. Sur la determination dune classe de fonctions analytiques par leurs valeurs dans un ensemble donne de poits. *in 'C.R. 6ieme Cong. Math. Scand. (Kopenhagen, 1925)', Gjellerups, Copenhagen*, pages 253–259, 1926.

[24] Z. Mao and J. Shen. Hermite spectral methods for fractional pdes in unbounded domains. *SIAM J. Sci. Comput.*, 39(5):1928–1950, 2017.

[25] F.J. Martin-Reyes. New proofs of weighted inequalities for the one-sided Hardy-Littlewood maximal functions. *Proc. Amer. Math. Soc.*, 117(3):691–698, 1993.

[26] M.K. Ng and J. Pan. Approximate inverse circulant-plus-diagonal preconditioners for toeplitz-plus-diagonal matrices. *SIAM J. Sci. Comput.*, 32(3):1442–1464, 2010.

[27] J. Pan, R. Ke, M.K. Ng, and H.-W. Sun. Preconditioning techniques for diagonal-times-toeplitz matrices in fractional diffusion equations. *SIAM J. Sci. Comput.*, 36(6):A2698–A2719, 2014.

[28] V.S. Rychkov. Littlewood-Paley Theory and Function Spaces with A_p^{loc} Weights. *Math. Nachr.*, 224:145–180, 2001.

[29] S.G. Samko, A.A. Kilbas, and O.I. Marichev. *Fractional Integrals and Derivatives: Theory and Applications*. Gordon and Breach Science Publishers, Yverdon,Switzerland, 1993.

[30] E. Sawyer. Weighted inequalities for the one-sided Hardy-Littlewood maximal functions. *Trans. Amer. Math. Soc.*, 297:53–61, 1986.

[31] J. Shen, T. Tang, and L. Wang. *Spectral Method: Algorithms, Analysis and Applications*. Springer-verlag. Berlin, Heidelberg, 2011.

[32] E.M. Stein. *Harmonic Analysis: Real-Variable Methods, Orthogonality and Oscillatory Integrals*. Princeton University Press, 1993.

[33] S. Takenaka. On the orthogonal functions and a new formula of interpolation. *Japanese J. Math.*, 2:129–145, 1926.

[34] T. Tao. *Nonlinear dispersive equations: Local and global analysis*. AMS, 2006.

[35] H. van der Vorst. *Iterative Krylov methods for large linear systems*. Cambridge University Press, Cambridge, UK, 2003.

[36] J. Weideman. Computing the Hilbert transform on the real line. *Math. Comp.*, 64(210):745–762, 1995.

[37] J. Weideman. Theory and applications of an orthogonal rational basis set. *in 'Proceedings South African Num. Math. Symp. 1994, Univ. Natal'*, 1995.

[38] H. Zhan, X. Jiang, C. Wang, and W. Fan. Galerkin-Legendre spectral schemes for nonlinear space fractional Schrödinger equation. *Numer. Algor.*, 79:337–356, 2018.